Contrib Mineral Petrol (2002) 143: 154–174
DOI 10.1007/s00410-001-0340-7

Jörg A. Pfänder · Klaus Peter Jochum · Ivan Kozakov
Alfred Kröner · Wolfgang Todt

Coupled evolution of back-arc and island arc-like mafic crust in the late-Neoproterozoic Agardagh Tes-Chem ophiolite, Central Asia: evidence from trace element and Sr–Nd–Pb isotope data

Received: 14 June 2001 / Accepted: 29 November 2001 / Published online: 2 March 2002
© Springer-Verlag 2002

Abstract We report major-element, trace-element and isotopic data of volcanic rocks from the late-Neoproterozoic (570 Ma) Agardagh Tes-Chem ophiolite in Central Asia, south-west of Lake Baikal (50.5°N, 95°E). The majority of samples are high-alumina basalts and basaltic andesites having island-arc affinities. They were derived from an evolved parental magma (Mg # ≥ 0.60, Cr∼180 ppm, Ni∼95 ppm) by predominantly clinopyroxene fractionation. The parental magma developed from a primary mantle melt by fractionation of about 12% of an olivine + spinel assemblage. The island-arc rocks have high abundances of incompatible trace elements (light rare-earth element abundances up to 100 times chondritic, chondrite-normalised $(La/Yb)_n = 14.6–5.1$) and negative Nb anomalies (Nb/La = 0.37–0.62), but low Zr/Nb ratios (7–14). Initial ϵ_{Nd} values are around +5.5, initial Pb isotopic compositions are $^{206}Pb/^{204}Pb = 17.39–18.45$, $^{207}Pb/^{204}Pb = 15.49–15.61$, $^{208}Pb/^{204}Pb = 37.06–38.05$. Enrichment of large-ion lithophile elements within this group is significant (Ba/La = 11–130). Another group of samples consists of back-arc basin-related volcanic rocks. They are most likely derived from the same depleted mantle source as the island-arc rocks, but underwent higher degrees of melting (8–15%) and are not influenced by slab components. They have lower abundances of incompatible trace elements, flat rare-earth element patterns [$(La/Yb)_n = 0.6–2.4$] and higher ϵ_{Nd} values (+7.8 to +8.5). Negative Nb anomalies are absent (Nb/La = 0.81–1.30), but Zr/Nb is high (21–48). At least three components are necessary to explain the geochemical evolution of the volcanic rocks: (1) an enriched (ocean island-like) component characterised by a high Nb concentration (up to 30 ppm), an absent negative Nb anomaly, a low Zr/Nb ratio (∼6.5), a low ϵ_{Nd} value (around 0), and radiogenic $^{206}Pb/^{204}Pb$, $^{207}Pb/^{204}Pb$ and $^{208}Pb/^{204}Pb$; (2) a back-arc basin component similar to N-MORB with a flat rare-earth element pattern and a high ϵ_{Nd} value (around +8.5); and (3) an island-arc component from a mantle source which was modified by the downgoing slab. Crystal fractionation superimposed on mixing and source contamination by subducted sediments is suitable to explain the observed geochemical data. The most likely geodynamic environment to produce these characteristics is a young, intra-oceanic island-arc system and an associated back-arc basin.

J.A. Pfänder (✉) · K.P. Jochum · W. Todt
Max-Planck-Institut für Chemie,
Postfach 3060, 55020 Mainz, Germany
E-mail: pfaender@uni-muenster.de
Tel.: +49-251-8336112

J.A. Pfänder · A. Kröner
Institut für Geowissenschaften,
Universität Mainz, 55099 Mainz, Germany

I. Kozakov
Institute of Precambrian Geology and Geochronology,
St. Petersburg, Russia

Present address: J.A. Pfänder
Institut für Mineralogie,
Universität Münster, Corrensstrasse 24,
48149 Münster, Germany

Editorial responsibility: J. Hoefs

Introduction

Geochemical, petrological and isotopic characteristics of volcanic rocks related to ophiolites are frequently used to reconstruct the geodynamic situation which led to the formation of the ophiolite, and to place constraints on the composition of the Earth's mantle for a distinct region and time interval (e.g. Swinden et al. 1990; Zimmer et al. 1995; Pedersen and Dunning 1997). Regional mantle sources, source contamination, melting processes, melt migration, and fractionation prior to ophiolite formation are a matter of intensive debate, and some of these processes obscure the primary signature of melts originally formed within the Earth's mantle. This is especially the case for island arc-related ophiolites, as isotopic and trace-element modifications of arc magmas

occur within several stages during magma genesis and ascent. Mantle-wedge heterogeneities may be an intrinsic feature or can be produced by element transfer from the downgoing slab to the mantle wedge via (1) fluids (Tatsumi 1989; Hawkesworth et al. 1997), (2) partial melts produced by melting of the downgoing slab (Rapp et al. 1999), (3) the accretion of unmolten or partially molten subducted sediments to the mantle wedge (Johnson and Plank 1999), or by a combination of these processes. As a consequence of fluid transfer from the slab to the mantle wedge, its solidus will be lowered leading to the formation of primary melts (Tatsumi 1989). Further modifications of these melts will occur on their way to the surface by the reaction with overlying mantle peridotite (Navon and Stolper 1987; Kelemen 1990), and by combined fractional crystallisation and assimilation of continental or pre-existing arc crust (e.g. DePaolo 1981). A detailed knowledge of these processes is thus essential for an understanding of regional mafic and continental crust formation.

Large volumes of continental and oceanic crust were accreted to the Siberian Craton during Neoproterozoic and Palaeozoic times, now represented by the Central Asian Mobile Belt (CAMB or Altaids; Sengör et al. 1993) which extends from the Pacific Ocean to the Urals (Fig. 1, inset). The origin and evolution of the CAMB is

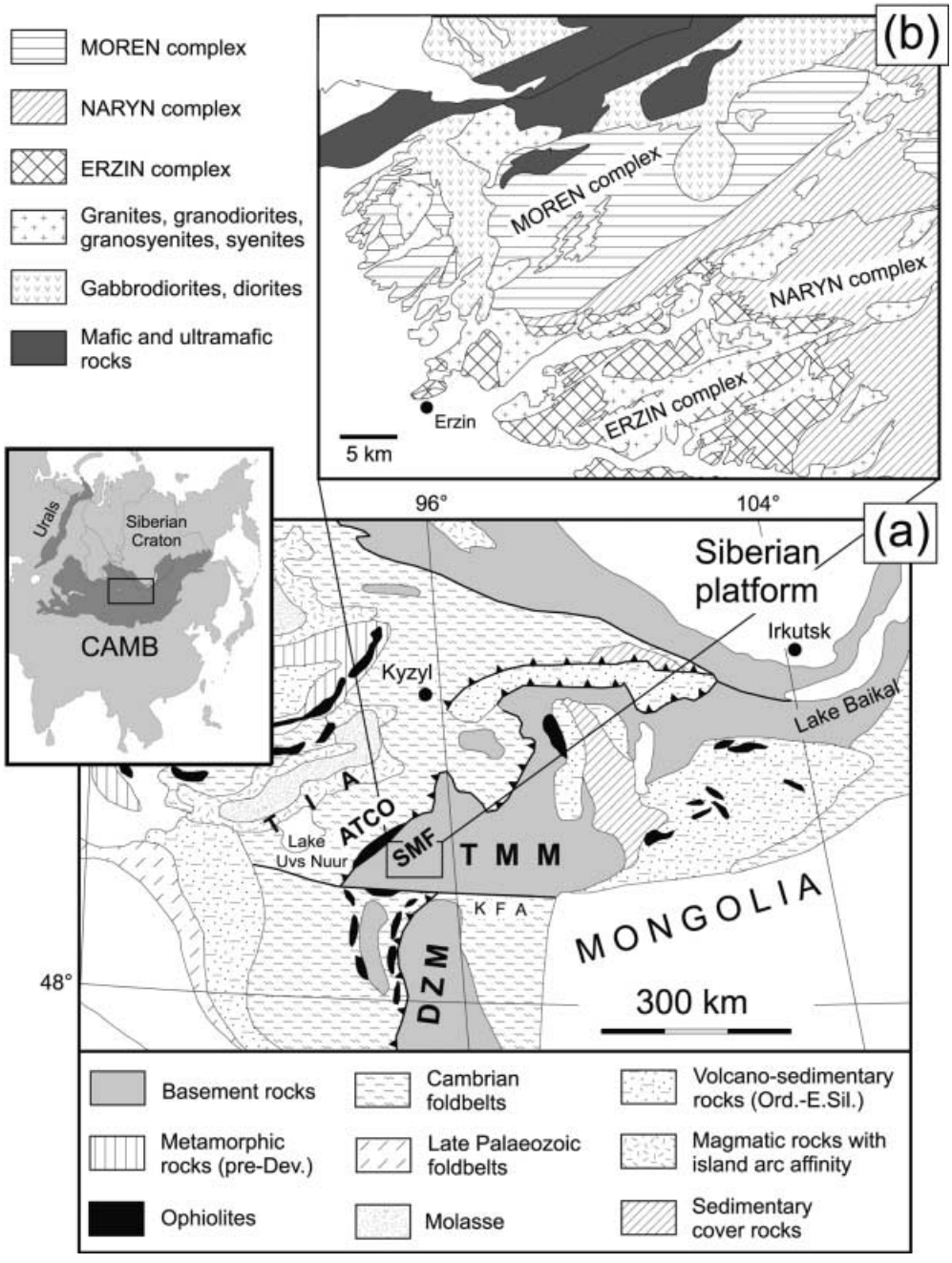

Fig. 1. **a** Central part of the Central Asian Mobile Belt (*CAMB*), showing main lithotectonic units. *ATCO* Agardagh Tes-Chem ophiolite, *TMM* Tuva-Mongolian microcontinent including the Sangilen massif (*SMF*) adjacent to the ophiolite, *TIA* Tannuola island arc, *DZM* Dzabkhanian microcontinent, *KFA* Khangay fault. *Inset* Geographical overview of Asia with exaggerated area framed (modified from Zonenshain et al. 1990). **b** Enlarged area showing the locations of the Moren, Naryn and Erzin complexes adjacent to the ophiolite (simplified after Salnikova et al. 2001)

poorly understood and controversially discussed (e.g. Sengör and Okurogullari 1991; Sengör et al. 1993). Basically, the CAMB represents an association of microcontinents which are interconnected by deformed Neoproterozoic to late-Palaeozoic subduction-accretion complexes (Sengör et al. 1993; Kuzmichev et al. 2001). These subduction-accretion complexes developed during the closure of the Palaeoasian Ocean (Belichenko et al. 1994; Melnikov et al. 1994; Khain et al. 1999). The microcontinents are assumed to be Precambrian in age (Coleman 1989; Mitrofanov and Kozakov 1993; Berzin et al. 1994) but their origin is contentious – they are fragments either from Gondwana (Mossakovsky et al. 1993; Didenko et al. 1994), or from the Siberian craton (Berzin et al. 1994), or from both.

Mafic crustal fragments are widespread within the CAMB where they roughly form EW-trending narrow belts (Zonenshain and Kuzmin 1978; Avdeyev 1984; Kepezhinskas 1986; Kepezhinskas et al. 1991; Kovalenko et al. 1996a, 1996b; Buchan et al. 2001). These belts are usually regarded as ophiolite zones, and thus are interpreted as remnants of the Palaeoasian Ocean (Khain et al. 1997), although their geodynamic origin, i.e., mid-ocean ridge-like oceanic crust or island arc-related crust, is poorly known. However, the ophiolites play an important role in deciphering the evolution of the CAMB because they are lithological markers of former plate boundaries (suture zones).

In this paper we describe the geochemical evolution of the late-Neoproterozoic (570 ± 2 Ma; Pfänder et al. 1998) Agardagh Tes-Chem ophiolite (ATCO), situated within the northern part of the CAMB (Fig. 1). This ophiolite is a well-preserved fragment of ultramafic to mafic crust and provides a unique opportunity to study crust formation processes operating on a large scale. In this context, the ATCO is particularly suitable to reveal the processes which initiated the evolution of the CAMB. We focus on volcanic rocks in which primary geochemical signatures were governed by partial melting, but were modified by crystal fractionation, mixing and contamination processes. We further constrain the geochemical and isotopic composition of the source of these rocks and outline a geodynamic framework suitable to explain the observed geochemical and isotopic data.

Geological setting

The ATCO marks the north-western border of the Tuva-Mongolian Microcontinent (TMM) which consists of several intrusive and metamorphic complexes (Kuzmichev et al. 2001; Salnikova et al. 2001; Fig. 1). To the SE and S of the ophiolite are the Moren, Erzin and Naryn complexes (Fig. 1; Kozakov 1986; Salnikova et al. 2001). The Moren complex consists of metatonalites, gneisses, migmatites, amphibolites, marbles, quartzites and minor ultramafic lenses. Kyanite-bearing gneisses indicate high-pressure metamorphic conditions (Kozakov 1986). The western part of the complex is intruded by early-Ordovician diorites and quartz diorites (Salnikova et al. 2001). The Erzin complex consists of garnet-bearing gneisses, migmatites, granulites and metavolcanic rocks (tholeiites, andesites, dacites). The Naryn complex consists of low-grade metapelites and calcareous quartzites. Carbonates are abundant and contain Middle-Riphean (~1,000 Ma) fossils (Mitrofanov and Kozakov 1993). All complexes belong to the Sangilen massif (SMF in Fig. 1a), which has traditionally been regarded as Precambrian basement of the TMM, comprising Palaeoproterozoic and Archaean rocks (Ez 1983; Ilyin 1990; Zonenshain et al. 1990). However, recent geochronological studies by Salnikova et al. (2001) yielded predominantly early-Palaeozoic ages for the metamorphic and intrusive rocks of the Moren, Naryn and Erzin complexes, making the existence of a Precambrian microcontinent questionable. To the north of the ophiolite succession lies the EW-striking Tannuola ridge (TIA in Fig. 1a), which represents a middle- to late-Ordovician island-arc assemblage (Zonenshain et al. 1990; Fedorovskii et al. 1995; Pfänder et al. 1998).

The ATCO can be subdivided into three main units. The south-western part (Agardagh unit, abbreviated as AD) consists mainly of variably serpentinised ultramafic rocks comprising dunite, harzburgite, wehrlite and pyroxenite. Small lenses of gabbro, gabbronorite and plagiogranite are also present. The AD unit is embedded within a tectonic mélange, consisting of schists, metasedimentary rocks, carbonates, cherts, sheared pillow lavas and basaltic rocks. The central part of the ATCO (Karachat unit, abbreviated as KA; Fig. 2) represents an intrusive body dominated by gabbros, hornblende-gabbros, gabbronorites and minor diorites. The north-eastern part of the ATCO (Tes-Chem unit, abbreviated as TC; Fig. 2) consists of the lower to intermediate part of a sheeted dyke complex, comprising microgabbros, massive basalts and basaltic andesites. Low-grade metamorphic pillow lavas occur as sheared bodies within the mélange associated to the TC unit. The samples analysed in this study are low-grade pillows and massive basalts from the AD unit (samples A22–A49; Table 1), massive basalts and basaltic dykes/sills from the KA unit (samples A39–A59; Table 1), and low-grade pillows, massive volcanics and microgabbros from the TC unit (samples T2–T44; Table 1).

Results

Major elements

Based on their SiO_2 concentration (Table 1), the volcanic rocks are subdivided into predominantly basalts and basaltic andesites with minor andesites, dacites and picrites. Na_2O and K_2O concentrations (Table 1) are not considered for classification, because alteration probably played a significant role in controlling the budget of alkaline elements within nearly all rocks. All samples except two (A7 and A59) are characterised by

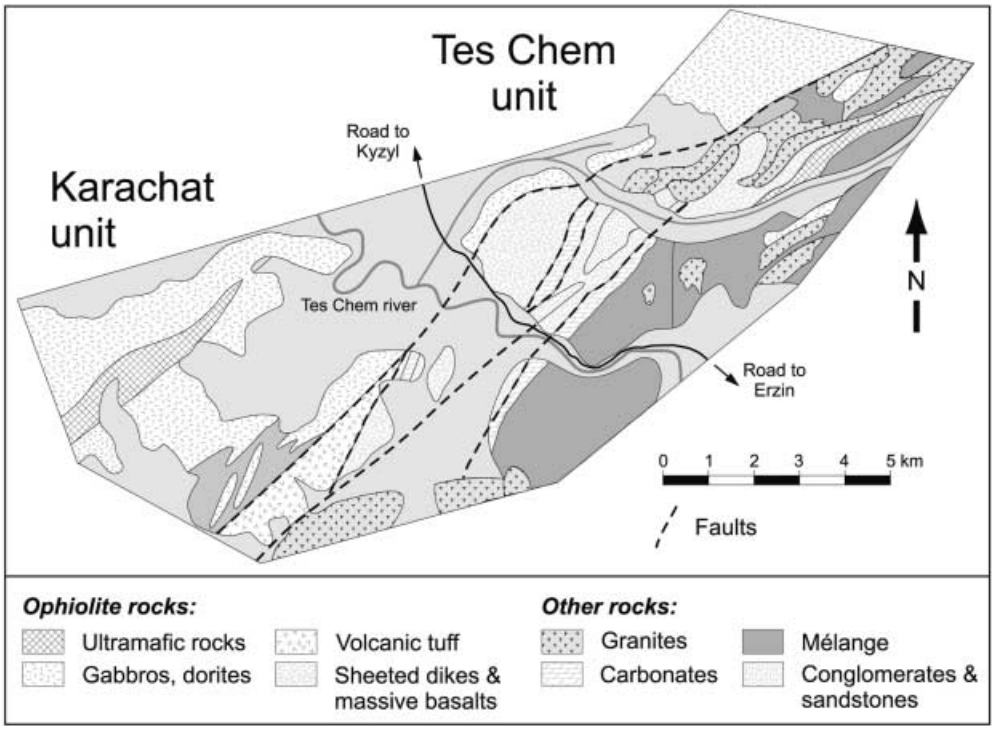

Fig. 2. Geological map of the north-eastern part of the Agardagh Tes-Chem ophiolite (ATCO), comprising the Karachat- and Tes-Chem units. The Agardagh unit lies further to the south-west and is not shown

calc-alkaline affinity. Mg numbers (Mg# = molar Mg/[Mg + Fe^{II}]) of volcanic rocks range from 0.48 to 0.67 for the TC-group rocks, from 0.54 to 0.69 for the KA-group rocks and from 0.49 to 0.73 for the AD-group rocks (Table 1). CaO decreases with decreasing MgO (Fig. 3a) for the TC- and KA-group rocks, whereas Al_2O_3 slightly increases (Fig. 3b). This may indicate that clinopyroxene (cpx) was a dominant phase during fractionation of KA- and TC-group parental melts. A large scatter in terms of major-element compositions for the AD-group volcanic rocks suggests a non-uniform origin of these samples. TiO_2 decreases with decreasing MgO for all samples (Fig. 4), but TiO_2 concentrations are generally high (0.5–2.9%, Table 1) and higher than in primitive ocean-floor basalts (~0.6–1%; Presnall and Hoover 1987) or in many island-arc basalts. The latter usually have $TiO_2 < 1\%$ (e.g. Woodhead et al. 1998) due to Ti retention in residual slab minerals (rutile, titanite; Brenan et al. 1994). By contrast, oceanic island basalts (OIB) tend to have higher TiO_2 (>2% TiO_2). In terms of TiO_2 concentration, most of the volcanic rocks are very similar to back-arc basin basalts (TiO_2~0.7–2%; Hawkins 1976; Hawkins and Melchior 1985; Eissen et al. 1991; Pearce et al. 1995) and mid-ocean ridge basalts (MORB average $TiO_2 = 1.6\%$; Hofmann 1988).

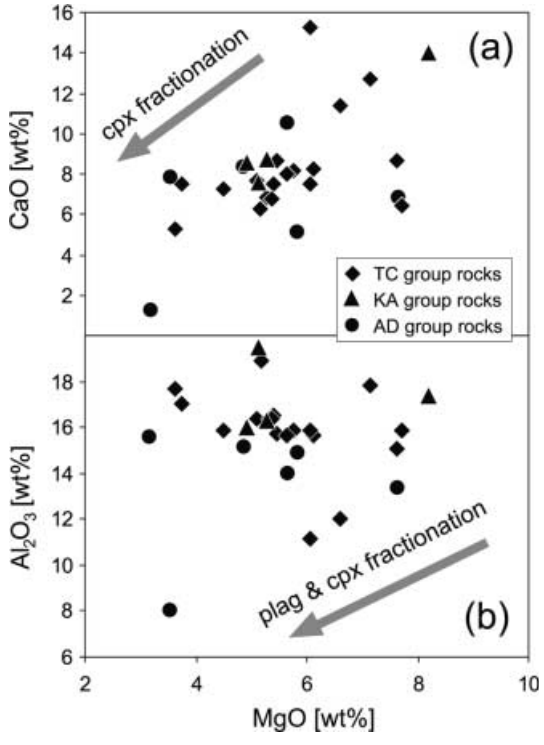

Fig. 3a, b CaO and Al_2O_3 vs. MgO for all volcanic rocks. **a** Decreasing CaO with decreasing MgO suggests clinopyroxene (cpx) fractionation. **b** Predominantly increasing Al_2O_3 concentrations suggest minor or absent plagioclase (plag) fractionation, except for some low-Al samples (*arrows* are schematic)

Trace elements

Compatible trace elements

Chromium and Ni concentrations (Table 1, Fig. 5a) in most of the volcanic rocks are low compared to primary basalts (Ni = 300–400 ppm, Cr = 300–500 ppm; Frey et al. 1978; Hess 1992). The concentrations of both elements are well correlated for most of the TC- and

Table 1. Major-element (wt%, LOI corrected) and trace-element (ppm) composition of volcanic rocks from the Agardagh Tes-Chem

Sample	Agardagh unit (AD)							Karachat unit (KA)					Tes-Chem unit (TC)	
Rock type[a]														
Group[b]	T97A22 ba BAB	T97A23 ba OIB	T97A24 da EX	T97A41 ba (p) BAB	T97A43 ba (p) BAB	T97A47 da EX	T97A49 an EX	T97A39 ba IA	T97A40 ba EX	T97A57 bs (d) D	T97A58 ba IA	T97A59 bt (d) D	T97T02 mg IA	T97T03 ba IA
SiO_2	52.59	52.08	69.53	53.47	53.39	64.18	55.08	52.22	52.74	48.73	52.10	42.48	52.55	53.16
Al_2O_3	14.98	8.65	8.13	15.19	13.42	15.65	14.08	16.02	19.47	16.09	16.31	17.42	16.34	16.34
Fe_2O_3	14.06	10.11	5.84	9.21	11.84	7.65	9.93	10.47	8.33	10.78	10.80	16.18	10.01	10.05
MnO	0.18	0.26	0.58	0.13	0.22	0.22	0.14	0.15	0.19	0.18	0.16	0.22	0.15	0.16
MgO	5.81	11.67	3.53	4.87	7.61	3.18	5.63	4.93	5.12	10.15	5.27	8.18	5.11	5.27
CaO	5.24	10.94	7.89	8.42	6.92	1.33	10.61	8.60	7.63	10.01	8.75	13.99	7.70	6.85
Na_2O	4.94	2.42	4.15	4.80	4.62	6.21	2.61	4.28	5.28	2.16	3.31	0.31	4.06	3.51
K_2O	0.62	0.87	0.32	0.30	0.29	0.97	0.65	1.11	0.22	0.07	0.93	0.05	1.74	2.44
TiO_2	1.72	2.90	0.35	1.45	1.69	0.78	1.20	1.48	0.90	0.76	1.51	0.60	1.31	1.31
P_2O_5	0.13	0.37	0.13	0.11	0.13	0.11	0.12	0.54	0.13	0.07	0.50	0.00	0.64	0.65
Cr_2O_3	0.01	0.02	0.01	0.05	0.00	0.01	0.04	0.01	0.00	0.08	0.01	0.00	0.02	0.02
NiO	0.00	0.02	0.01	0.01	0.00	0.00	0.02	0.00	0.00	0.02	0.01	0.01	0.01	0.01
LOI	3.57	3.60	4.09	2.40	2.13	2.36	1.93	1.33	2.71	1.68	2.44	2.58	1.79	2.95
Total	100.28	100.31	100.48	98.00	100.13	100.29	100.13	99.82	100.01	99.11	99.67	99.44	99.65	99.78
FeO*	10.75	7.73	4.46	7.04	9.06	5.85	7.60	8.01	6.37	8.25	8.26	12.37	7.66	7.68
Mg#	0.49	0.73	0.59	0.55	0.60	0.49	0.57	0.52	0.59	0.69	0.53	0.54	0.54	0.55
Rb	9	9	4	3	5.77	17	7.68	16.5	6	0.389	13.1	0.292	16.9	38
Sr	129	110	106	82	223	139	261	613	368	177	508	114	604	547
Ba	73	336	103	55	54	185	151	327	81	28	259	11	450	634
Y	39	23	21	32	43	34	17	23.3	8	15.6	20.7	2.03	33.5	30
Zr	95	199	62	90	96	112	58	128	23	36.1	113	0.53	143	175
Hf	2.98	5.76	1.88	2.99	2.60	–	1.79	–	–	1.29	–	–	–	–
Nb	3	29	3	4	2	4	5	9.59	2	0.820	11.5	0.039	12.6	13
U	0.137	0.816	0.792	0.090	0.095	–	0.134	0.470	–	0.088	0.490	0.004	0.539	–
Th	0.170	2.46	1.45	0.186	0.141	–	0.395	2.17	–	0.155	1.41	0.046	2.04	–
Pb	0.880	2.92	4.11	1.43	1.72	4	3.31	1.94	3	3.22	3.15	0.858	6.00	9
Sc	40	23	17	41	34	22	21	34	18	38	28	61	26	25
V	458	238	86	308	405	115	155	246	200	247	241	713	202	206
Cr	20	122	111	404	7	51	302	76	25	604	84	9	116	115
Co	41	41	28	41	30	15	40	19	30	43	29	61	32	30
Ni	26	104	79	89	18	24	187	33	24	179	42	43	56	63
Cu	9	1	20	56	25	32	58	25	32	51	81	220	50	58
Zn	53	71	56	78	68	91	90	70	77	88	109	76	101	99
Ga	20	11	10	14	15	17	18	19	19	15	19	14	20	19
La	3.70	26.5	8.54	3.08	3.49	–	4.79	21.0	–	2.46	21.2	0.19	31.0	–
Ce	12.2	61.0	30.5	9.06	11.9	–	11.4	48.6	–	6.93	46.2	0.29	59.9	–
Pr	1.96	8.13	2.48	1.49	1.98	–	1.53	6.25	–	1.04	5.51	0.04	9.54	–
Nd	9.87	29.9	9.26	9.06	12.1	–	8.09	29.9	–	5.01	27.4	0.19	36.1	–
Sm	3.62	6.56	2.56	3.26	4.51	–	3.03	6.63	–	1.64	6.07	0.11	7.37	–
Eu	1.52	3.46	1.17	0.98	1.31	–	1.50	2.00	–	0.63	1.77	0.15	2.26	–
Gd	4.04	8.21	4.30	3.28	4.50	–	3.01	6.35	–	2.47	5.51	0.26	7.08	–
Tb	–	–	–	–	–	–	–	0.91	–	0.39	0.81	0.06	0.99	–
Dy	4.90	5.31		4.39	6.21	–	2.65	5.46	–	2.69	4.71	–	6.13	–
Ho	1.13	1.07	0.75	0.96	1.43	–	0.53	1.07	–	0.52	0.92	0.09	1.23	–
Er	3.71	2.81	2.35	2.69	3.85	–	1.44	3.00	–	1.74	2.52	0.28	2.95	–
Tm	–	–	–	–	–	–	–	0.37	–	–	0.32	–	0.45	–
Yb	4.72	2.42	2.95	2.48	3.84	–	1.41	2.37	–	1.41	2.05	0.32	3.16	–
Lu	–	–	–	–	–	–	–	0.34	–	0.19	0.29	0.03	0.37	–

[a] *bs* basalt, *ba* basaltic andesite, *an* andesite, *da* dacite, *bt* basanite, *mg* microgabbro, *p* pillow, *d* dyke
[b] *IA* island arc, *BAB* back-arc basin, *OIB* ocean-island affinity, *D* dyke, *EX* exotic sample. Rb, Sr, Sm and Nd by TIMS, all other trace *XRF*

KA-group rocks (except A57, T6 and T7; Fig. 5a), suggesting a common parental magma and substantial cpx and/or combined olivine and spinel fractionation. A few samples are characterised by relatively high Mg# (0.67–0.73; MgO up to 11.7 wt%) and high Ni and Cr concentrations (up to 187 and 604 ppm respectively, Fig. 5b). These samples may represent less fractionated, primary melts. On the other hand, due to the generally large scatter, it is unlikely that all volcanic rocks were derived from one single parental melt by simple fractionation processes.

Incompatible trace elements

Primitive mantle-normalised trace-element concentrations of selected samples from all three units are shown in Fig. 6 (primitive mantle = PRIMA; Hofmann 1988).

ophiolite. FeO* was calculated treating all iron as FeO and assuming that $FeO/(FeO + Fe_2O_3) = 0.85$

T97T04 bs IA	T97T05 bs IA	T97T06 ba IA	T97T07 mg D	T97T14 ba IA	T97T15 an IA	T97T16 bs IA	T97T17 ba IA	T97T18 mg IA	T97T20 ba IA	T97T31 ba IA	T97T39 bs IA	T97T40 bs IA	T97T41 bs IA	T97T42 bs IA	T97T43 bs IA	T97T44 bs IA
51.21	50.43	52.51	42.59	52.21	56.07	49.12	53.12	55.34	52.15	53.09	51.19	49.97	50.32	50.27	50.98	48.78
12.04	11.13	15.07	17.84	16.49	17.68	19.13	15.88	17.00	15.73	16.39	15.84	15.62	15.65	15.66	15.83	15.87
11.11	10.08	8.75	18.17	11.15	8.65	11.00	11.24	8.40	10.47	11.23	11.90	12.50	12.00	12.04	12.01	12.44
0.16	0.16	0.17	0.23	0.16	0.14	0.18	0.17	0.12	0.18	0.17	0.17	0.19	0.18	0.19	0.19	0.22
6.59	6.06	7.63	7.16	5.41	3.63	5.17	4.50	3.74	5.46	5.37	5.75	5.64	5.63	6.11	6.05	7.71
11.42	15.22	8.70	12.73	7.49	5.31	6.28	7.27	7.52	8.66	6.80	8.13	7.98	8.03	8.24	7.53	6.43
4.34	4.42	3.08	0.11	4.38	6.00	5.70	3.64	3.57	3.44	3.68	3.28	3.30	3.35	3.06	3.26	3.78
0.29	0.24	2.82	0.25	1.34	0.88	0.80	1.63	1.57	0.85	1.65	1.03	1.00	1.16	1.30	1.17,	1.221.22
2.84	2.50	0.76	0.56	0.97	0.80	1.88	1.63	1.16	1.57	1.24	1.76	1.92	1.83	1.76	1.74	1.96
0.32	0.29	0.27	0.00	0.36	0.34	0.52	0.77	0.51	0.64	0.45	0.75	0.78	0.77	0.73	0.75	0.77
0.02	0.02	0.05	0.01	0.01	0.01	0.01	0.01	0.01	0.02	0.02	0.02	0.02	0.02	0.02	0.02	0.02
0.01	0.01	0.01	0.00	0.00	0.00	0.00	0.00	0.00	0.01	0.00	0.01	0.01	0.01	0.01	0.01	0.01
4.10	6.59	3.51	3.15	7.32	3.93	5.52	1.43	1.73	1.31	4.84	1.93	3.08	2.31	2.99	2.21	2.77
100.35	100.55	99.80	99.65	99.96	99.52	99.78	99.88	98.93	99.18	100.09	99.84	98.91	98.94	99.40	99.54	99.20
8.50	7.71	6.69	13.90	8.52	6.62	8.41	8.60	6.42	8.01	8.59	9.10	9.56	9.18	9.21	9.18	9.51
0.58	0.58	0.67	0.48	0.53	0.49	0.52	0.48	0.51	0.55	0.53	0.53	0.51	0.52	0.54	0.54	0.59
4	3	37	8.29	23.0	11.6	15.7	22	27.4	11.4	23	17.7	18	21	21.9	21	14.4
380	365	648	117	766	749	1,024	565	558	744	1,413	704	721	724	652	668	635
96	75	364	36	1,266	860	345	575	574	399	1,036	356	357	477	379	355	611
23	21	17	1.88	17.4	15.9	24.2	34	22.4	25.3	20	31.9	34	34	34.8	34	36.5
168	147	76	1.13	76.6	99.0	143	187	152	121	147	146	174	176	144	172	151
–	–	–	–	–	3.81	3.47	–	4.14	–	–	–	–	–	3.57	–	3.83
26	23	3	0.034	11.3	11.3	11.4	14	10.9	11.1	14	13.5	13	13	13.3	13	12.9
–	–	–	0.030	1.53	1.78	1.03	–	0.735	0.463	–	0.434	–	–	0.377	–	0.449
–	–	–	0.011	5.35	5.03	2.71	–	2.55	1.79	–	1.45	–	–	1.27	–	1.13
5	3	10	2.71	10.5	27.7	6.31	9	6.60	3.44	19	3.24	6	5	5.64	5	6.32
33	30	29	70	29	19	18	28	27	25	33	28	28	29	30	26	29
301	271	223	782	263	160	199	270	199	221	272	249	270	255	256	251	278
170	136	368	9	79	47	58	33	42	155	140	140	138	131	165	159	130
39	36	32	57	30	21	33	29	14	24	32	33	36	33	35	36	38
89	71	80	15	26	17	32	22	21	67	38	57	52	49	79	62	52
112	83	75	195	30	28	49	57	112	28	58	62	51	33	38	48	48
87	74	72	103	92	75	74	104	80	107	103	103	115	123	128	125	113
17	15	16	18	20	19	18	21	19	19	22	21	21	19	19	19	19
–	17.5	–	0.28	30.4	25.1	23.0	–	23.3	22.9	–	27.8	–	–	21.1	–	23.3
–	41.1	–	0.43	56.2	52.5	50.3	–	48.8	46.2	–	68.7	–	–	44.9	–	55.1
–	–	–	0.06	7.18	7.29	7.26	–	7.10	7.57	–	9.12	–	–	7.44	–	8.41
–	23.5	–	0.25	29.1	31.0	32.7	–	30.4	35.8	–	36.4	–	–	35.2	–	37.9
–	6.79	–	0.13	5.96	6.30	6.74	–	6.27	7.13	–	7.82	–	–	7.62	–	8.28
–	1.56	–	0.17	2.15	1.86	1.94	–	2.07	2.11	–	2.72	–	–	1.88	–	2.22
–	5.75	–	0.25	5.68	–	–	–	–	6.50	–	–	–	–	–	–	-
–	–	–	–	0.69	0.74	0.85	–	1.02	0.88	–	1.04	–	–	0.87	–	1.06
–	4.97	–	–	3.98	–	–	–	–	5.34	–	5.88	–	–	6.95	–	6.92
–	–	–	0.08	0.71	0.64	0.90	–	0.95	1.03	–	1.17	–	–	0.98	–	1.07
–	2.55	–	0.28	1.79	1.53	2.53	–	2.58	2.56	–	3.20	–	–	2.68	–	2.96
–	–	–	–	0.24	–	–	–	–	0.36	–	0.48	–	–	–	–	-
–	1.64	–	0.33	1.49	1.74	2.57	–	3.08	2.53	–	3.00	–	–	2.80	–	3.31
–	0.17	–	0.03	0.18	0.25	0.36	–	0.38	0.30	–	0.46	–	–	0.37	–	0.42

elements by MIC-SSMS or ICP-MS (samples A39, A58, T02, T14, T20, T39) except Sc, V, Cr, Co, Ni, Cu, Zn, Ga and underlined by

All TC-group samples (Fig. 6a) are characterised by negative Nb anomalies with relatively uniform Nb/La ratios (Nb/La = 0.37–0.62, except T7: 0.12). Nb/U ratios are more variable (6.4–35), indicating variable enrichment of U relative to N-MORB (Nb/U = 49; data for N-MORB from Hofmann 1988). Lead anomalies are also variable (Ce/Pb = 1.9–21, except T7: 0.2), but are overall positive compared to N-MORB (Ce/Pb = 25). Th/U ratios within this group vary between 2.5 and 3.9 with an average of 3.3 ± 0.5 (1σ). Sample T7 is also characterised by a negative Nb and a positive Pb anomaly, but displays a significant depletion in incompatible trace elements relative to primitive mantle and N-MORB. All TC samples are characterised by slightly positive Sr and negative Ti anomalies. KA-group samples (Fig. 6b) have also negative Nb anomalies (Nb/La = 0.20–0.54; Nb/U = 9.1–23), but span a wider range in trace-element concentrations than TC-group rocks.

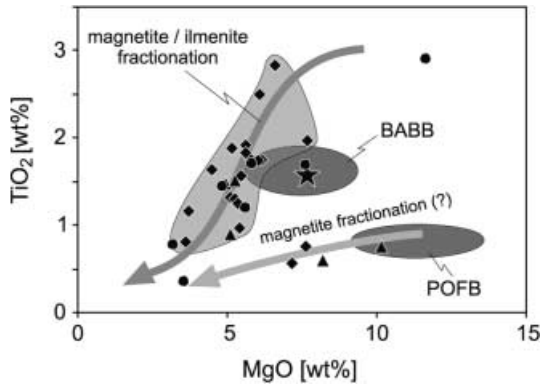

Fig. 4. TiO_2 vs. MgO. Decreasing TiO_2 with decreasing MgO indicates magnetite-titanomagnetite and/or ilmenite fractionation accompanying olivine-clinopyroxene fractionation (*arrows*, schematic). TiO_2 concentrations for most of the samples are higher than in primitive ocean-floor basalts (*POFB*; Presnall and Hoover 1987) but resemble back-arc basin basalts (*BABB*; Eissen et al. 1995), although the variation is significantly larger (symbols as in Fig. 3). *Star* Average MORB (Hofmann 1988)

However, the most enriched KA samples resemble the TC-group rocks and thus most likely represent the same source. Lead anomalies are similar to the TC-suite rocks (Ce/Pb = 2.2–25, except A59: 0.4). However, Th/U ratios are more variable than in TC-group samples (Th/U = 1.8–10.5). AD-group rocks (Fig. 6c) are heterogeneous compared to KA- and TC-group rocks, with one sample (A23) having an oceanic island-like (''OIB-like'') trace-element pattern (Fig. 6c). This sample is characterised by enrichment of Nb (Nb/La = 1.1; Nb/U = 37) and depletion of Pb (Ce/Pb = 21). Two AD-group rocks are metapillows which are very similar in trace-element composition to N-MORB (Fig. 6d). Th/U ratios within all AD-group rocks vary between 1.2 and 3.0 with an average of 2.1 ± 0.7 (1σ) and thus are significantly lower than in TC-group rocks.

Zr/Nb ratios of volcanic rocks from all three units vary between 6.4 and 48 and correlate with Nb concentrations (see below). Ba/La ratios do not differ significantly between different units (average value for TC~23, for KA~25, for AD~19), but are higher than in primitive mantle (Ba/La = 10) and N-MORB (Ba/La = 3.6). This indicates an enrichment of large-ion lithophile elements (LILE) within all rocks. Zr/Hf ratios vary between 26 and 41 with an average of 34 ± 5 (N-MORB = 35; PRIMA = 36). Ti/V ratios for all rocks are between 19 and 57 (except A23, A59 and T7), and thus are more in the range of back-arc basin (BAB) basalts or MORB (typically between 20 and 50) than within the range of many island-arc basalts (typically < 20; Shervais 1982).

Rare-earth elements

Based on their chondrite-normalised rare-earth element (REE) abundances (Fig. 7), the volcanic rocks are

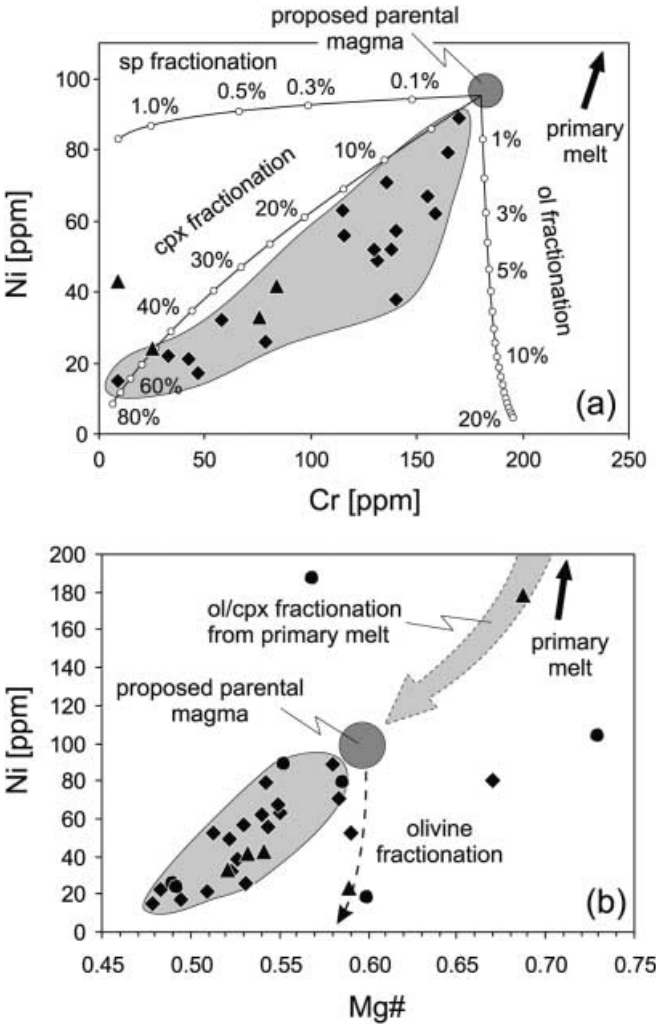

Fig. 5. **a** Ni vs. Cr in TC- and KA-group volcanic rocks (*rhombs* TC group, *triangles* KA group). Ni and Cr are well correlated, indicating either substantial clinopyroxene fractionation or combined olivine and spinel fractionation (Rayleigh fractionation, partition coefficients from 1994; *numbers* give amount of phase fractionated). **b** Ni vs. Mg# of all volcanic rocks, including AD-group rocks (*circles*). The proposed composition of the parental magma is Mg# ~0.60, Ni ~95 ppm, Cr ~180 ppm

subdivided into three groups. All TC-group samples (except T7; Fig. 7a) and two KA volcanic rocks (A39 and A58; Fig. 7b) show a significant enrichment in light (L) REE relative to chondrite and heavy (H) REE. Chondrite-normalised $(La/Yb)_n$ ratios for this group are between 14.6 and 5.1, whereas $(Sm/Nd)_n$ is nearly constant (0.61–0.67). Eu anomalies are negligible or absent. Based on the REE content, this group of rocks is very similar to unusually enriched island-arc basaltic rocks from the Lesser Antilles Islands (Fig. 7a, b). These rocks are low-Mg calcic basalts generated from picritic parental melts by high-level fractionation of plagioclase, augite, olivine, and titano-magnetite (Thirlwall and Graham 1984). In the following we refer to the LREE-enriched group as island arc-related rocks (IA rocks).

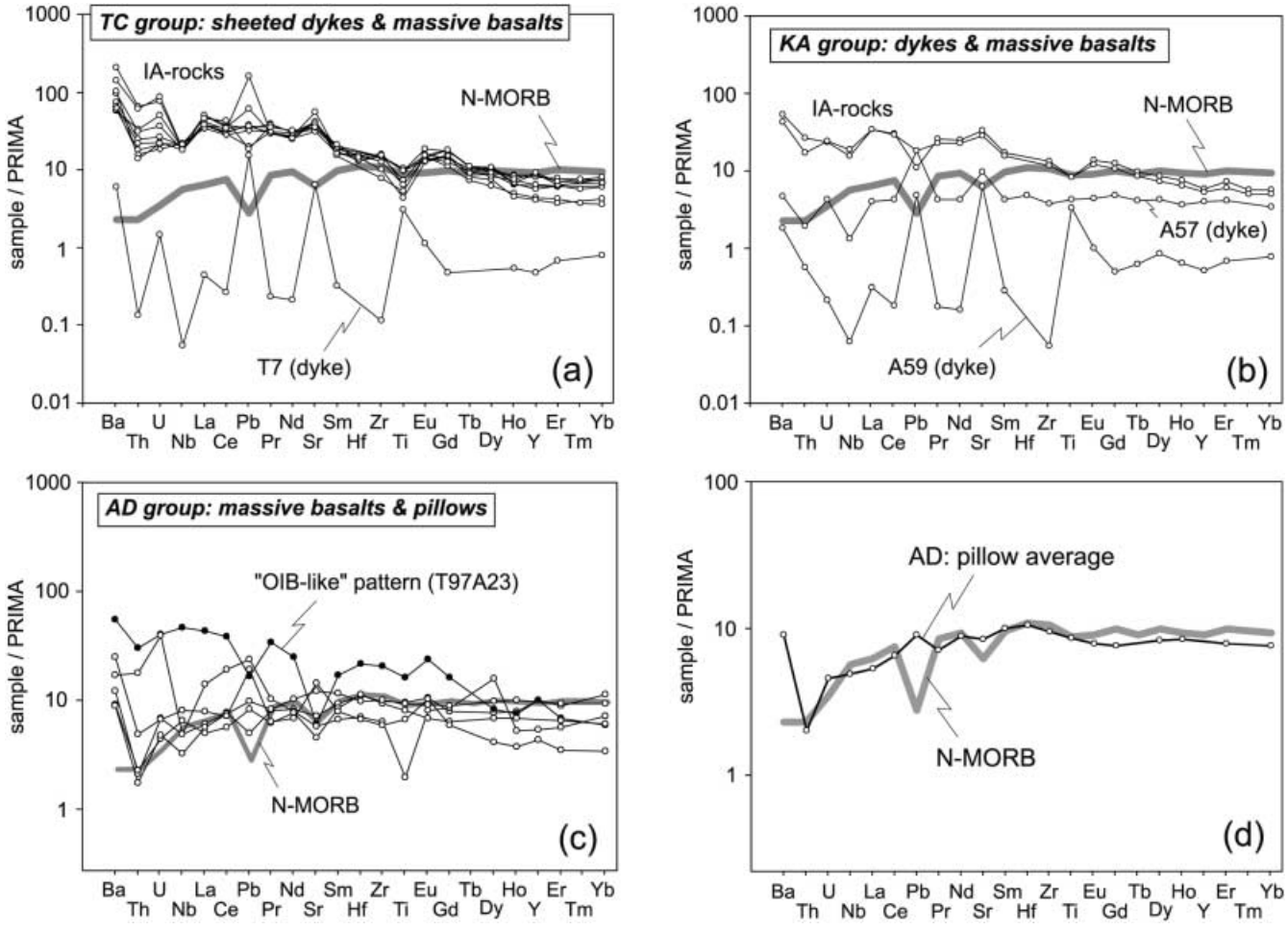

Fig. 6a–d. Concentrations of incompatible trace elements for selected samples, normalised to primitive mantle values (Hofmann 1988). **a** TC-group rocks have negative Nb anomalies and are strongly enriched in highly incompatible trace elements relative to N-MORB (except T7). Pb anomalies are variable. **b** KA-group rocks have negative Nb and Pb anomalies. One sample is more depleted with a positive Pb anomaly. Sample A59 represents a dyke and strongly resembles sample T7 of the TC group. **c** AD-group rocks are heterogeneous with one sample having an "OIB-like" pattern (absent negative Nb anomaly, negative Pb anomaly). **d** Average of two AD-group metapillows (note the similarity to N-MORB). Generally, TC- and KA-group volcanic rocks are very similar, but different to AD-group volcanic rocks. Samples T7 and A59, and probably A57, are dykes and are characterised by completely different trace-element characteristics. *Shaded curves* N-MORB for comparison (data from Hofmann 1988). Note different scales

The second group comprising all AD volcanic rocks is characterised by flat REE patterns (Fig. 7c; except the "OIB-like" sample A23) with $(La/Yb)_n = 0.6–2.4$, $(La/Sm)_n = 0.5–1.0$, and $(Sm/Nd)_n = 0.8$ and 1.1. Eu anomalies are absent or slightly positive. Although the general pattern within this group is the same, absolute abundances vary significantly by a factor of about 2 for the LREE, and of about 4 for the HREE. Despite the variability in absolute REE abundances and nonparallel REE patterns, we refer to this group as back-arc basin-related samples in the following (BAB rocks). The assumption of a back-arc or even open-basin origin of at least some of these samples is justified not only by trace-element data (Figs. 6d, 7c) but also by field relationships and isotopic results discussed below. Nevertheless, we emphasise that the BAB rocks may even represent fragments of "true" mid-ocean ridge- (MOR) related mafic rocks as the transition from back arc to open marine is difficult to constrain geochemically.

The third group is represented by only two samples (dykes T7 and A59; Fig. 7a, b) and is characterised by a depleted but U-shaped LREE pattern with $(La/Yb)_n = 0.4$ and 0.6, $(La/Sm)_n = 1.1$ and 1.4, and $(Sm/Nd)_n = 1.5$ and 1.8. Positive Eu anomalies as well as La and Ce enrichments are due to the presence of feldspar phenocrysts.

Isotopic data

Sr and Nd whole-rock isotopic compositions and Sr, Rb, Nd and Sm concentrations of selected samples are listed in Table 2. Initial $^{87}Sr/^{86}Sr$ ratios (calculated for an age of 570 Ma) vary between 0.70294 and 0.70590, with the highest values lying close to the range given for seawater 570 Ma ago (0.7065 and 0.7075; Jacobsen and Kaufman 1999).

Initial ϵ_{Nd} values (570 Ma) of samples from all three units are also given in Table 2 and are shown in Fig. 8. The values span a large range from –0.6 for the least radiogenic sample (A24) to +8.5 for the most radiogenic sample (A22), with the latter value being close to the 570 Ma depleted mantle value of +8.75 (linear evolution model after Goldstein et al. 1984). Both samples belong to the AD section, whereas the KA- and TC-group rocks are more uniform in their Nd isotopic composition ($\epsilon_{Nd}(570) = +5.5$ to $+7.7$ and $+1.9$ to $+5.9$, respectively), whereby the majority of samples have initial ϵ_{Nd} values around +5.5.

Based on the classification in IA and BAB rocks, the IA rocks have intermediate but variable initial ϵ_{Nd} values between +1.9 and +6.0 (average: +4.6), whereas the BAB rocks have higher initial ϵ_{Nd} values between +7.7 and +8.5 (average: +8.0). The U-shaped, REE-depleted samples (dykes T7 and A59) have intermediate initial ϵ_{Nd} values of +5.1 and +5.5, suggesting that these two samples were derived from the same source as the IA rocks. However, the most unradiogenic samples (initial ϵ_{Nd} values between –0.6 and +2.4) have both flat and enriched REE patterns, ruling out a simple genetic relationship. Generally, the large variation of initial ϵ_{Nd} and the poor linear correlation in terms of $^{143}Nd/^{144}Nd$ vs. $^{147}Sm/^{144}Nd$ within and between the different units rule out a comagmatic evolution (linear regression of all samples would yield an insignificant errorchron with an age of 630 ± 130 Ma, MSWD = 147, $R^2 = 0.84$).

Measured and age-corrected Pb isotopic compositions of samples from all three units are given in Table 3 and shown in Fig. 9. Age correction to 570 Ma was done using high-precision Th, U and Pb concentrations determined by isotope dilution MIC-SSMS. The TC- and KA-group rocks have age-corrected $^{207}Pb/^{204}Pb$ and $^{206}Pb/^{204}Pb$ ratios of 15.49 to 15.61 and 17.39 to 18.46 respectively. By contrast, the AD-group rocks display a wider range in age-corrected $^{207}Pb/^{204}Pb$ and $^{206}Pb/^{204}Pb$ of 15.53 to15.78 and 17.19 to 20.33 respectively (Fig. 9a). This is consistent with the wider range in initial ϵ_{Nd} values for this group. Considering measured $^{208}Pb/^{204}Pb$ vs. $^{206}Pb/^{204}Pb$ ratios, the TC- and KA-group rocks (including IA rocks) are well correlated (Fig. 9b), whereas the AD-group rocks (including BAB rocks) plot to the right of this array.

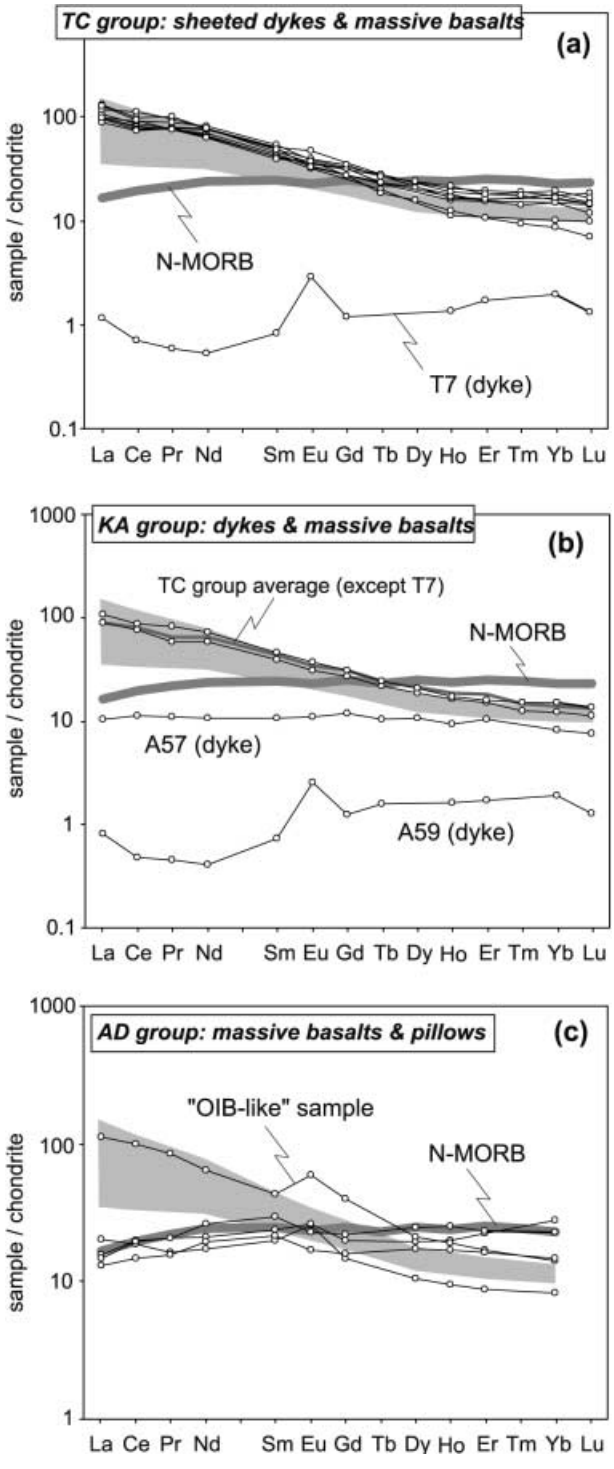

Fig. 7a–c. Chondrite-normalised REE composition of volcanic rocks. **a** TC-group rocks are strongly enriched in LREE compared to N-MORB, but depleted in HREE (except strongly depleted dyke sample T7). **b** KA-group rocks split into enriched massive basalts, identical to TC-group rocks, and one flat and one LREE-depleted dyke sample. **c** AD-group rocks are more heterogeneous but tend to have flat REE patterns similar to MORB, except one sample termed ''OIB-like''. *Shaded field* Enriched basaltic rocks from the Lesser Antilles island arc (data from Thirlwall and Graham 1984; normalising values from Sun and McDonough 1989, data for N-MORB from Hofmann 1988)

Discussion

Alteration, metamorphism and element mobility

All volcanic rocks analysed during the course of this study were altered by hydrothermal and low-grade metamorphic processes. In order to address questions on mantle-source geochemistry and magmatic processes based on trace-element and isotope data, the effects of

Table 2. Rb–Sr and Sm–Nd data of volcanic rocks from the Agardagh Tes-Chem ophiolite

	Rb (ppm)	Sr (ppm)	$^{87}Rb/^{86}Sr$	$(^{87}Sr/^{86}Sr)_m$[a]	$(^{87}Sr/^{86}Sr)_i$[b]	Sm (ppm)	Nd (ppm)	$^{147}Sm/^{144}Nd$	$(^{143}Nd/^{144}Nd)_m$[a]	$(^{143}Nd/^{144}Nd)_i$[b]	$(\epsilon_{Nd})_{570}$
Agardagh unit (AD)											
T97A22	–	–	–	–	–	3.62	9.87	0.2219	0.513168 ± 8	0.512340	8.5
T97A23	–	–	–	–	–	6.56	29.9	0.1328	0.512522 ± 10	0.512027	2.4
T97A24	–	–	–	–	–	2.56	9.26	0.1668	0.512498 ± 7	0.511876	–0.6
T97A41	–	–	–	–	–	3.26	9.06	0.2173	0.513114 ± 8	0.512303	7.8
T97A43	5.77	222.9	0.0749	0.705898 ± 12	0.705290	4.51	12.1	0.2245	0.513147 ± 11	0.512309	7.9
T97A49	7.68	260.5	0.0853	0.705791 ± 13	0.705098	3.03	8.09	0.2263	0.512753 ± 8	0.511909	0.1
Karachat unit (KA)											
T97A39	16.5	612.9	0.0778	0.704487 ± 11	0.703855	6.63	29.9	0.1339	0.512710 ± 13	0.512211	6.0
T97A57	0.389	177.5	0.0063	0.703311 ± 11	0.703260	1.64	5.01	0.1975	0.513035 ± 12	0.512298	7.7
T97A58	13.1	507.8	0.0745	0.704409 ± 8	0.703804	6.07	27.4	0.1340	0.512661 ± 12	0.512161	5.0
T97A59	0.292	114.1	0.0074	0.703460 ± 10	0.703400	0.11	0.19	0.3561	0.513517 ± 13	0.512187	5.5
Tes-Chem unit (TC)											
T97T02	16.9	603.6	0.0810	0.704620 ± 14	0.703963	7.37	36.1	0.1232	0.512657 ± 5	0.512198	5.7
T97T04		–	–	–	–	5.99	26.2	0.1381	0.512651 ± 5	0.512136	4.5
T97T05		–	–	–	–	5.21	23.1	0.1365	0.512652 ± 5	0.512143	4.7
T97T07	8.29	117.3	0.2045	0.704600 ± 12	0.702938	0.126	0.250	0.3038	0.513298 ± 12	0.512163	5.1
T97T14	23.0	766.0	0.0867	0.705774 ± 18	0.705070	5.96	29.1	0.1238	0.512482 ± 6	0.512020	2.3
T97T15	11.6	748.9	0.0446	0.705485 ± 10	0.705123	6.30	31.0	0.1231	0.512461 ± 5	0.512001	1.9
T97T16	15.7	1,024	0.0442	0.704831 ± 12	0.704472	6.74	32.7	0.1245	0.512626 ± 13	0.512162	5.0
T97T18	27.4	558.2	0.1422	0.704732 ± 7	0.703577	6.27	30.4	0.1248	0.512651 ± 15	0.512185	5.5
T97T20	11.4	744.0	0.0442	0.704503 ± 13	0.704144	7.13	35.8	0.1205	0.512656 ± 3	0.512207	5.9
T97T39	17.7	703.9	0.0729	0.704489 ± 15	0.703897	7.82	36.4	0.1301	0.512607 ± 5	0.512122	4.3
T97T42	21.9	652.5	0.0971	0.704603 ± 8	0.703815	7.62	35.2	0.1309	0.512655 ± 9	0.512166	5.1
T97T44	14.4	635.2	0.0653	0.704534 ± 14	0.704003	8.28	37.9	0.1321	0.512645 ± 16	0.512153	4.9

[a]Measured values, error: in-run precision from individual ratios ($2\sigma_m$), given are the last digits of the reported value
[b]Initial values calculated for an age of 570 Ma

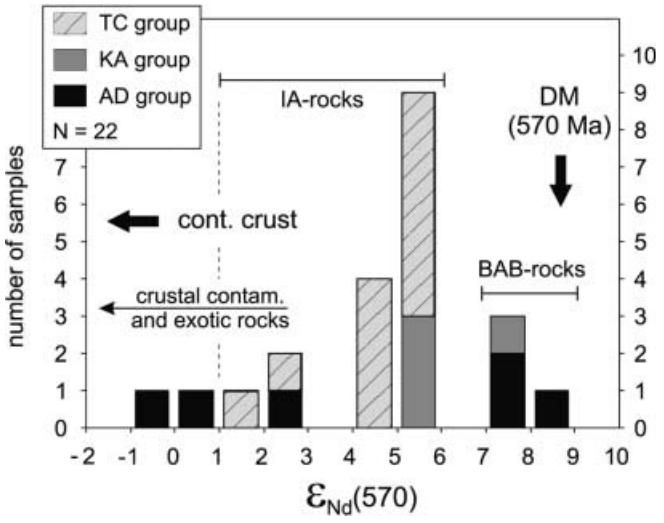

Fig. 8. Distribution of initial ϵ_{Nd} values for samples from all three units. AD-group rocks have the largest range (from –1 up to +9) and include highly depleted BAB rocks (metapillows) and enriched fragments associated with the mélange. TC- and KA-group rocks are more uniform with a maximum of around +5.5. Although KA volcanic rocks tend to be more radiogenic than TC-group rocks, both groups mainly represent IA rocks. *DM* gives the depleted mantle value 570 Ma ago, old continental crust plots outside the given range

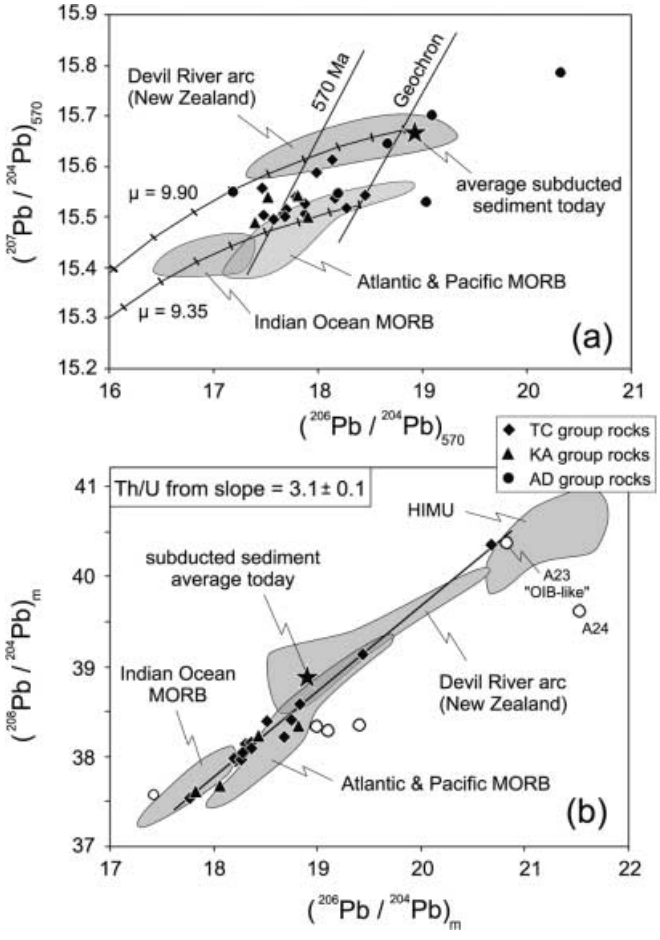

Fig. 9a, b. Pb isotopic composition of volcanic rocks from all three units. **a** Age-corrected $^{207}Pb/^{204}Pb$ vs. $^{206}Pb/^{204}Pb$ ratios plot between two Pb evolution lines with $\mu = 9.35$ and $\mu = 9.90$ respectively (tick distance is 200 Ma, for details see text). Also shown are the geochron and the 570 Ma primary isochron. Data for Atlantic, Pacific and Indian ocean MORB are from Ito et al. (1987) and are recalculated to 570 Ma using $\mu = 8.92$. Also shown are age-corrected data from the slightly younger (500 Ma) Devil River arc system in New Zealand (Münker 2000), which is an intra-oceanic arc back-arc system. **b** Measured $^{208}Pb/^{204}Pb$ vs. $^{206}Pb/^{204}Pb$ is linearly correlated for the IA rocks (*filled symbols*), with the slope giving a time-integrated Th/U ratio for the source of 3.1. The BAB rocks (*open circles*) are scattered but more radiogenic in $^{206}Pb/^{204}Pb$, indicating a slightly lower Th/U ratio of their source. HIMU data from Chauvel et al. (1992), sediment data from Plank and Langmuir (1998)

hydrothermal alteration and low-grade metamorphism have to be considered. A general consensus exists that transition metals (e.g. Cr, Ni), middle (M) REE, HREE, high-field strength elements (HFSE) as well as Th and Ti are relatively immobile during low-temperature alteration (e.g. Ludden et al. 1982; Staudigel et al. 1996). By contrast, alkali metals (e.g. Na, K, Rb), alkaline-earth metals (e.g. Sr, Ba) as well as LREE and to a minor extent U are known to be considerably mobile in fluids (Staudigel et al. 1996). For the ATCO volcanic rocks, there is a good linear correlation between immobile Th and fluid mobile U ($R^2 = 0.936$), indicating that variations in U concentrations are not dominated by hydrothermal and metamorphic processes. On the other hand, Pb isotope duplicate analyses measured on individual rock chips of selected samples show considerable variations (Table 3). However, these variations are restricted to $^{206}Pb/^{204}Pb$ and $^{208}Pb/^{204}Pb$ ratios, whereas for $^{207}Pb/^{204}Pb$ ratios conventional and triple spike analyses are identical within error. Alteration, however, most likely would affect all Pb isotope ratios. Therefore, we attribute the variations in $^{208}Pb/^{204}Pb$ and $^{206}Pb/^{204}Pb$ ratios within individual rock chips to radioactive in-growth from heterogeneously distributed Th and U which were derived from the subducting slab during magma genesis. If incompletely homogenised, this will yield large variations in $^{208}Pb/^{204}Pb$ and $^{206}Pb/^{204}Pb$ ratios, whereas $^{207}Pb/^{204}Pb$ ratios will be nearly unaffected duo to already low abundances of ^{235}U 570 Ma ago. From this we conclude that even Pb, as moderately fluid mobile element, is only little affected by alteration and low-grade metamorphism. Strontium is also mobile during hydrothermal alteration and metamorphism, and for mantle-derived rocks a shift in Sr concentration caused by seafloor hydrothermal alteration is typically accompanied by elevated $^{87}Sr/^{86}Sr(t)$ ratios relative to $\epsilon_{Nd}(t)$. In terms of their initial $^{87}Sr/^{86}Sr$ ratios vs. ϵ_{Nd} (570 Ma), the volcanic rocks and dykes of the ATCO plot to the right of the recent mantle array and to the lower right of the MORB field recalculated to 570 Ma. Some initial $^{87}Sr/^{86}Sr$ ratios are shifted to higher values for a given ϵ_{Nd} (570), which is most likely caused by moderate seawater alteration ($^{87}Sr/^{86}Sr$ in seawater ~570 Ma ago was between about 0.7065 and 0.7075; Jacobsen and Kaufman 1999). Therefore, Sr isotopic

Table 3. Pb isotopic data of volcanic rocks from the Agardagh Tes-Chem ophiolite

	Measured values				Corrected to 570 Ma[a]		
	$^{208}Pb/^{204}Pb$	$^{207}Pb/^{204}Pb$	$^{206}Pb/^{204}Pb$	$^{207}Pb/^{206}Pb$	$^{208}Pb/^{204}Pb$	$^{207}Pb/^{204}Pb$	$^{206}Pb/^{204}Pb$
Agardagh unit (AD)							
T97A22	38.28	15.60	19.11	0.8162	37.91	15.54	18.19
T97A23	40.37	15.80	20.83	0.7586	38.69	15.70	19.09
T97A24	39.61	15.85	21.53	0.7365	38.91	15.78	20.33
T97A41	38.34	15.55	19.41	0.8010	38.09	15.53	19.04
T97A43	38.33	15.66	19.00	0.8242	38.18	15.64	18.68
T97A49	37.57	15.56	17.42	0.8932	37.35	15.55	17.19
Karachat unit (KA)							
T97A39	38.34	15.57	18.82	0.8276	36.24	15.49	17.39
T97A57	37.67	15.51	18.06	0.8588	37.59	15.50	17.90
T97A58	38.24	15.59	18.43	0.8462	37.40	15.54	17.52
T97A59	37.62	15.54	17.83	0.8717	37.52	15.54	17.80
Tes-Chem unit (TC)							
T97T02	37.97	15.53	18.21	0.8529	37.34	15.50	17.69
T97T05	40.35	15.70	20.68	0.7589	–	–	–
T97T07	37.55	15.52	17.77	0.8735	37.54	15.52	17.70
T97T14	38.13	15.61	18.31	0.8524	37.18	15.56	17.46
T97T15	38.15	15.61	18.36	0.8502	37.81	15.59	17.99
T97T16	39.13	15.60	19.43	0.8028	38.30	15.54	18.46
T97T18	38.58	15.58	18.84	0.8271	37.85	15.54	18.18
T97T20	38.03	15.55	18.27	0.8514	37.06	15.50	17.48
T97T39	38.09	15.54	18.36	0.8464	37.25	15.50	17.58
T97T42	37.97	15.53	18.26	0.8502	37.55	15.51	17.88
T97T44	38.22	15.54	18.69	0.8318	37.88	15.52	18.27
Pb triple spike duplicates							
T97T02	37.9848 ± 0.0051	15.5364 ± 0.0016	18.1921 ± 0.0013	0.854019 ± 0.000028	37.355	15.506	17.671
T97T15	38.3919 ± 0.0043	15.6365 ± 0.0013	18.5137 ± 0.0011	0.844606 ± 0.000024	38.052	15.614	18.138
T97T16	38.4088 ± 0.0035	15.5978 ± 0.0011	18.7532 ± 0.0010	0.831741 ± 0.000018	37.601	15.541	17.795
T97T44	38.0478 ± 0.0054	15.5507 ± 0.0017	18.2842 ± 0.0014	0.850504 ± 0.000030	37.714	15.526	17.871

[a]Corrected for in-situ decay of Th and U using high-precision Th, U and Pb concentrations determined by isotope dilution MIC-SSMS. The error of the triple spike analyses is given as two sigma of the mean ($2\sigma_m$) and was computed from the in-run precision values of the spiked and unspiked runs of each sample. The error for all other ratios is $\pm 10^{-3}$

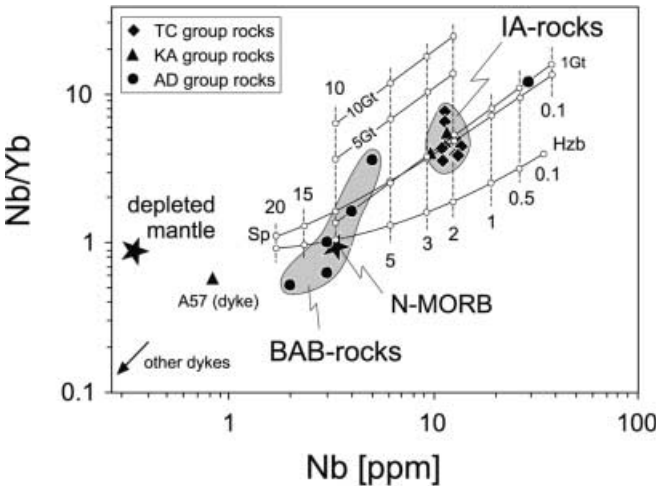

Fig. 10. Nb/Yb vs. Nb concentration. IA rocks have higher Nb/Yb ratios and higher Nb concentrations than BAB rocks, due to lower degrees of melting, assuming the same source. Curves are calculated melting curves for spinel peridotite (*Sp*), harzburgite (*Hzb*), garnet peridotite containing 10% garnet (*10 Gt*), 5% garnet (*5 Gt*), and 1% garnet (*1 Gt*; for details see text and Table 4). *Numbers* denote degree of melting (non-modal batch melting, partition coefficients from Bédard 1994, and Johnson 1998). Nb concentration is nearly independent of source composition but varies with degree of melting. Nb/Yb ratios are governed by the modal composition of the source

compositions are not further considered. Similar to Sr, Ba is a mobile element and sensitive to hydrothermal alteration and fluid flux (Staudigel et al. 1996). Nevertheless, we use Ba/La ratios to quantify LILE enrichment in the different rock suites. This is justified by a fairly good linear correlation between Ba and Th concentrations ($R^2 = 0.820$). Nevertheless, Ba anomalies, especially in low-concentration samples such as the BAB rocks and dykes (Fig. 6a, b), may reflect some degree of alteration. In conclusion, we predominantly use the more immobile elements (HFSE, Th, MREE and HREE) as well as Nd and Pb isotopes, which have shown to be less affected within the ATCO volcanic rocks.

Parental magma(s) and fractional crystallisation

Low abundances of Cr and Ni and moderately to low Mg# in most of the volcanic rocks, particularly the TC- and KA-group samples (i.e. IA rocks, Fig. 5), indicate substantial fractionation to produce the parental magma of these rocks from a primary melt. Using the Mg# and Cr and Ni concentrations, we infer the composition of the parental magma to have been as follows: Mg#≥0.60, Cr≥180 ppm and Ni≥95 ppm (Fig. 5). Decreasing the Cr and Ni concentrations of a mantle-derived primary melt (~500 ppm Cr and ~400 ppm Ni; Frey et al. 1978) to these values requires fractionation of about 12% solid phases with a composition of 95% olivine and 5% spinel (assuming Rayleigh fractionation, partition coefficients from Bédard 1994, and Conrad and Kay 1984). This amount seems reasonable with respect to the Mg# of the inferred parental magma (e.g. fractionation of about 15% olivine with an average Fo = 0.81 reduces the Mg# of a melt from 0.70 to 0.61). Therefore, fractionation of olivine and spinel from a primary melt could produce the parental magma from which the TC- and KA-group rocks further developed. The assumption of predominantly olivine (and ± spinel) crystallisation is justified since primary melts have only olivine on their liquidus at moderate to low pressures (Hess 1992). As demonstrated by Heath et al. (1998) who investigated calc-alkaline series from the Lesser Antilles, the assumption of olivine and Cr-spinel as liquidus phases is also valid for primary melts related to arc environments.

Proceeding from the parental magma inferred above, fractionation of ~60% cpx or ~1% spinel and ~15% olivine is required to fit the observed range in Mg#, Cr and Ni within the volcanic rocks themselves (Fig. 5). Due to the occurrence of cpx phenocrysts, the absence of olivine phenocrysts, the decreasing CaO with decreasing MgO (Fig. 3a), and the elevated SiO_2 concentration and the quartz normative character of most of the volcanic rocks, we prefer the assumption of predominantly cpx fractionation from the parental magma. Negative Ti anomalies and decreasing TiO_2 with decreasing MgO (Fig. 4) further show that magnetite/ilmenite fractionation also played a role during the evolution of the volcanic rocks. Increasing Al_2O_3 with decreasing MgO (Fig. 3b) indicates that plagioclase was not a dominant liquidus phase during the fractionation of the volcanic series. This is further supported by absent Eu anomalies within most samples from all three units (Figs. 6, 7). On the other hand, positive Sr anomalies in the IA rocks (Fig. 6) suggest plagioclase accumulation. However, as

Table 4. Source and melt modes used for melting calculations

Source modes					Melt modes					Source
Ol	Opx	Cpx	Sp	Gt	Ol	Opx	Cpx	Sp	Gt	
57	25	16	2	0	–7	25	80	2	0	Spinel lherzolite[a] (cpx out after 20% melting)
60	20	10	0	10	4	–19	105	0	10	Garnet peridotite[b] (cpx out after 10% melting)
83	15	0	2	0	35	63	0	2	0	Harzburgite[c] (opx out after 24% melting)

[a]Woodhead et al. (1993)
[b]Johnson (1998)
[c]Kelemen et al. (1990)

Sr/Nd is positively correlated with Th/La, indicating variable amounts of slab-derived components within the IA rocks, we attribute the positive Sr anomalies to slab components rather than to plagioclase accumulation. Exceptions are the highly depleted dike samples with strongly positive Eu and Sr anomalies. These dykes are mostly microgabbros and thus dominated by plagioclase accumulation.

Degree of melting

Estimating the degree of melting implies several problems due to variable enrichment effects of the magma source caused by subduction-related processes. It is well known that the budget of hydrophile elements (Rb, K, Sr, Ba, U, Pb) in the mantle wedge is controlled by fluids released from the dehydrating slab (Peacock 1993; Ryan et al. 1996; Regelous et al. 1997; Johnson and Plank 1999). On the other hand, the inventory of more immobile, incompatible elements (e.g. Th) may be controlled by melts formed from the slab itself (Peacock et al. 1994), or from subducted sediments, or from sediments directly accreted to the mantle wedge (Hawkesworth et al. 1997; Johnson and Plank 1999). Although all IA rocks display significant negative Nb anomalies (Fig. 6a, b), absolute abundances of Nb are about a factor of 3 higher than in BAB rocks (predominantly AD-group rocks) and in N-MORB (Fig. 10). Therefore, the negative Nb anomalies indicate an enrichment of LILE relative to Nb and other HFSE rather than depletion of these elements by subduction-related processes such as HFSE retention in residual mantle or slab minerals (e.g. rutile). This is consistent with experimental results which suggest that rutile saturation in island-arc magmas is difficult to achieve, thus making the existence of HFSE-retarding phases in the source region of arc magmas unlikely (Ryerson and Watson 1987; Ionov and Hofmann 1995). We therefore assume that the Nb contribution from the slab to the source region of the IA rocks is negligible, making Nb a potential indicator to estimate the degree of melting of the primary mantle wedge. Similar to the HFSE, the HREE are regarded as conservative elements, for which the contribution from the slab to the mantle wedge is also minimal (Pearce and Peate 1995). Therefore, we used Nb–Yb systematics to calculate the composition of melts produced by different degrees of melting and variable source compositions (Fig. 10), applying the equation for non-modal batch melting (Shaw 1970; Albarède 1995). Starting concentrations of Nb and Yb in the source are taken as 0.35 ppm and 0.39 ppm respectively. These values are reasonable estimates for the depleted upper mantle and are derived from the N-MORB composition of Hofmann (1988), assuming that N-MORB is produced by 10% batch melting of depleted mantle peridotite. These concentrations are in good agreement with the depleted mantle concentrations given by McKenzie and O'Nions (1991, 1995; Nb = 0.39 ppm, Yb = 0.35 ppm). Mantle and corresponding melt modes are taken from Woodhead et al. (1993) for spinel lherzolite, from Johnson (1998) for garnet peridotite, and from Kelemen et al. (1990) for harzburgite (Table 4). Additionally, initial garnet abundances are varied from the original composition of 10% (Johnson 1998) to 5% and 1%. The lower garnet modes were compensated by olivine.

Our calculations indicate that the mantle source was either a moderately depleted spinel lherzolite similar to the recent MORB source mantle, or a more refractory garnet peridotite which underwent higher proportions of former melt extraction. Relatively low Nb/Yb ratios rule out a garnet proportion of more than 1–2%. Independent of the source composition, the degree of melting was low for the IA rocks (about 2–3%). This is in good agreement with the degree of melting predicted for hydrous melting above subduction zones (2–8%; Davies and Bickle 1991), although our estimate is at the lower limit of this range. This may indicate a generally low fluid flux, as the degree of melting above subduction zones is proportional to the fluid flux from the slab (Stolper and Newman 1994). For the BAB rocks the degree of melting was probably higher (8–15%), assuming the same source. The dyke samples of the KA region (including T7) plot off the general trend for IA and BAB rocks (Fig. 10). Due to their extremely low Nb concentrations and very low Nb/Yb ratios, they cannot be derived from the same source as IA and BAB rocks and thus may represent later-stage intrusion events of unknown age.

Source composition

High initial ϵ_{Nd} values (up to +8.5; Table 2) in the metapillows of the AD section (BAB rocks in Fig. 8) indicate the existence of a long-term depleted mantle beneath Central Asia 570 Ma ago. Compared to the global evolution of Nd isotopes (e.g. Stein and Hofmann 1994), these values are close to the Nd isotopic composition of the depleted mantle 570 Ma ago, assuming that the depleted mantle evolution is defined by the upper limit of global initial ϵ_{Nd} values vs. time. By contrast, the ϵ_{Nd} values of the IA rocks scatter around +5.5 (Table 2, Fig. 8) and lie on the Nd evolution line for major orogens (see Stein and Hofmann 1994). Therefore, the IA rocks may either be attributed to a different source, which then would be less depleted than the upper mantle (e.g. a mixed primordial and depleted mantle source, as suggested by Stein and Hofmann 1994), or may be the result of mixing and/or assimilation processes, whereby material derived from older continental crust lowers the initial ϵ_{Nd} values. Due to the variation of initial ϵ_{Nd} values of the IA rocks, and due to the mixing relationships described below, we favour the assumption of a similar source for BAB and IA rocks. This source was a long-term depleted mantle.

Pb isotopic compositions (Table 3) constrain the μ value (=present-day $^{238}U/^{204}Pb$) of the mantle source to have been 9.35 as a lower limit (Fig. 9a). We calculated this value by applying a two-stage Pb evolution model, following Stacey and Kramers (1975) for the first step and assuming an age of the Earth of 4.57 Ga. The μ value of 9.35 is slightly higher than the depleted-mantle estimate of Doe and Zartman (1979; $\mu = 8.92$) but nevertheless underlines the existence of a depleted mantle source beneath Central Asia as derived from Nd isotopes. Furthermore, the μ value lies close to the more recent estimate of Hofmann (2001; $\mu = 9.26$), based on the average composition of MORB and assuming a single-stage Pb evolution and an age of the Earth of 4.43 Ga. $^{206}Pb/^{204}Pb$ ratios of all samples, except the highly heterogeneous AD-series samples, lie within the range of age-corrected Atlantic, Pacific and Indian MORB (Fig. 9a; MORB data from Ito et al. 1987; recalculated to 570 Ma using $\mu = 8.92$). However, considering $^{207}Pb/^{204}Pb$ ratios there is an excess in ^{207}Pb compared to recalculated MORB samples. This excess probably reflects the existence of small amounts of old crustal material, either within the source itself and derived from the subducted slab, or assimilated by ascending melts. An excess in radiogenic ^{207}Pb in arc magmas was also described by Münker (2000; Fig. 9a) for the 500-Ma-old Devil River arc system in New Zealand. He showed that this excess was produced by subducted sediments derived from an Archaean source.

From the well-defined correlation between $^{208}Pb/^{204}Pb$ vs. $^{206}Pb/^{204}Pb$ within the IA rocks (Fig. 9b), we deduce a time-integrated Th/U ratio of their source of 3.1 ± 0.1 (1σ; disregarding the AD series rocks). Compared to the present-day depleted mantle (Th/U~2.5, Galer and O'Nions 1985), this indicates a slight long-term excess in ^{208}Pb over ^{206}Pb, which we also attribute to older crustal components with a long-term increased Th/U relative to the depleted mantle. By contrast, the BAB rocks plot significantly to the right of the correlation defined by the IA rocks, indicating an excess in ^{206}Pb and thus a significantly lower time-integrated Th/U ratio for their source.

Mixing relationships vs. single parental melt

Although Cr and Ni correlations (Fig. 5) as well as Nb/Yb systematics (Fig. 10) allow the assumption of a common parental magma for most of the volcanic rocks, other trace-element and isotopic characteristics require additional processes to have taken place during their evolution. In terms of Zr/Nb vs. Nb concentration, the BAB rocks are characterised by high Zr/Nb ratios (up to 50; Fig. 11). The IA rocks as well as the metapillows from the TC mélange and sample A23 have lower Zr/Nb ratios but higher Nb concentrations (Fig. 11). Crystal fractionation fails to explain the correlation between the different groups of samples, as this process is not sufficient to produce such a large range in Zr/Nb ratios. This is demonstrated in Fig. 11 by the calculated fractionation trend for cpx, which produces a Zr/Nb variation being an order of magnitude too low to fit the observed data. Fractionation of other mafic phases will yield similar trends (e.g. 50% Rayleigh fractionation of a primary magma having Zr/Nb = 30 would lower this ratio to about 28 for cpx fractionation and to about 25 for amphibole fractionation). Partial melting is suitable to explain some of the variations within the IA and low-Zr/Nb BAB rocks as described previously and as shown by the partial melting curve for spinel peridotite in Fig. 11 (non-modal batch melting, parameters as given in Table 4). However, partial melting is not sufficient to explain the entire range in Zr/Nb ratios. Therefore, we suggest a mixing relationship superimposed on partial melting and fractional crystallisation to explain the variation in Zr/Nb ratios. Bulk mixing between a high-Nb component (represented by the "OIB-like" sample A23) and a highly depleted primary melt, having a low Nb concentration and a high Zr/Nb ratio (represented by metapillow A43), is shown in Fig. 11. According to this, the admixture of up to about 10% of the "OIB-like" component explains the Zr/Nb variation within the entire suite of BAB rocks. As discussed in Münker (2000), melts with low Zr/Nb ratios but high Nb concentrations may also result from melting of a subducted slab, where Nb behaves much more incompatibly than Zr. We cannot rule out this assumption and therefore underline that the component termed "OIB-like" could also be a melt derived from slab melting. For example, 3% modal batch melting of a N-MORB-like slab consisting of garnet amphibolite having 10% garnet results in a melt having ~30 ppm Nb and Zr/Nb~9 (Münker 2000). This is very close to sample A23. However, the "OIB-like" samples occur in the mélange of the ophiolite and are related to the forearc region of the subduction-accretion system. Therefore, they may represent fragments of an accreted, "OIB-like" terrane rather than melts derived from a recently subducted slab, where the thermal regime is unlikely to produce significant amounts of slab-derived melts.

Isotopic data provide further constraints on mixing relationships. Radiogenic lead $(^{208}Pb/^{206}Pb)^*$ is negatively correlated with initial $^{143}Nd/^{144}Nd$ (Fig. 12). This indicates the contamination of primary magmas with an old crustal component, as high $(^{208}Pb/^{206}Pb)^*$ is observed in reservoirs having a high Th/U over time, i.e. in the continental crust. No significant differences exist whether age-corrected $(^{208}Pb/^{206}Pb)^*$ is used or not, indicating that differences in radiogenic Pb compositions derived from different Th/U ratios reflect long-living source heterogeneities. This is also evident from initial $^{207}Pb/^{204}Pb$, in which higher values correspond to lower initial ϵ_{Nd}. The AD pillows A22, A41 and A43 have the lowest $(^{208}Pb/^{206}Pb)^*$ ratios (0.877–0.913) and the most radiogenic $^{143}Nd/^{144}Nd$ ($\epsilon_{Nd} = +7.8$ to $+8.5$). As shown above, these samples are thought to represent BAB-related melts from a depleted mantle source for which

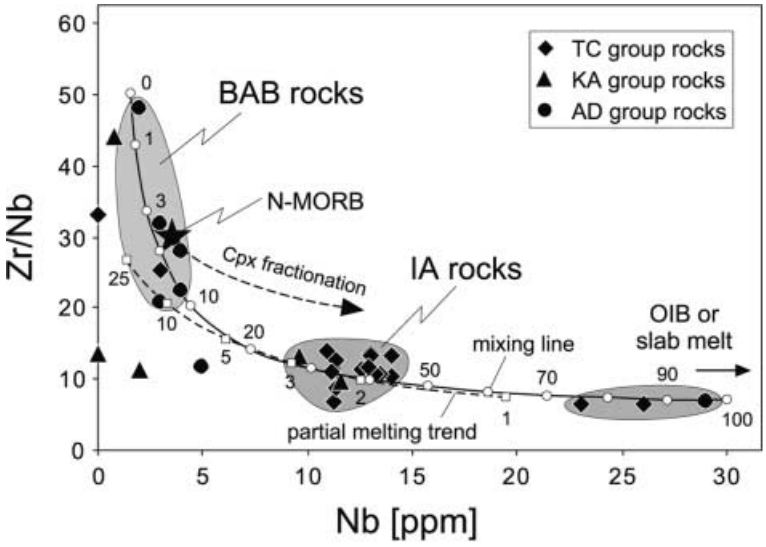

Fig. 11. Zr/Nb vs. Nb concentration. Variation of Zr/Nb ratios is an order of magnitude too large to be explained by fractional crystallisation (e.g. cpx fractionation, length of *arrow* corresponds to 85% Rayleigh fractionation). Partial melting also fails to explain the whole range in Zr/Nb vs. Nb (lower *dashed line*, *numbers* denote degree of melting. Therefore, we infer a mixing relationship between a Nb-rich component (''OIB-like'' melt) and a highly depleted melt, superimposed on the partial melting trend connecting the IA and low-Zr/Nb BAB rocks. The mixing line was calculated by bulk mixing between the sample having the highest Nb concentration (''OIB-like'' sample A23) and the sample having the highest Zr/Nb ratio (metapillow A43). *Numbers* are mixing proportions in %

contamination or crustal assimilation played a minor role. On the other hand, the island-arc rocks have significantly lower initial $^{143}Nd/^{144}Nd$ ($\epsilon_{Nd} = +1.9$ to $+5.9$) and slightly higher $(^{208}Pb/^{206}Pb)^*$ ratios (Fig. 12), indicating the involvement of older continental material during their evolution. To place constraints on the potential contaminant, we calculated a simple bulk mixing relationship between a primary melt (represented by the BAB pillow lavas) and a sediment component. Due to the lack of geochemical data on regional sediments, we used the average composition of subducted sediments given by Plank and Langmuir (1998). As shown in Fig. 12, the IA rocks plot along the calculated mixing line, making subducted sediments with moderate to low ϵ_{Nd} values the most likely contaminant during the evolution of the IA rocks. This observation is consistent with mixing relationships derived from Zr/Nb systematics, but makes the involvement of an ''OIB-like'' component during melt generation unnecessary. Therefore, the ''OIB-like'' samples possibly represent isolated rock fragments accreted to the forearc region as described above, rather than components involved during magma genesis. This assumption is confirmed by the scatter in $(^{208}Pb/^{206}Pb)^*$ vs. $^{143}Nd/^{144}Nd$ for three of the six AD-group rocks (Fig. 12), which suggests that they do not originate from a single source but rather represent different lithotectonic units.

Crustal assimilation vs. source contamination

Several authors have estimated the flux and timing of material transfer from the slab to the mantle wedge (e.g. Morris et al. 1990; Hawkesworth et al. 1997; Regelous et al. 1997; Elliot et al. 1997; Johnson and Plank 1999), and constrained the behaviour of different elements during mass transfer. For example, Johnson and Plank (1999) pointed out that Rb, Sr, Ba and Pb are highly fluid mobile elements whereas Th is mobilised only by melting of subducted sediments. Because most of the investigated samples were altered during low-grade metamorphism, the influence of fluid phases during melt generation is difficult to assess for the ATCO. On the other hand, as outlined above, low degrees of melting for the IA rocks suggest low fluid fluxes from the slab. Additionally, we infer from the correlation between initial $(^{208}Pb/^{206}Pb)^*$ vs. $^{143}Nd/^{144}Nd$ (Fig. 12) that the source contaminant was at least partly a sedimentary component. However, as shown in Fig. 12, up to 40% sediment admixture to a primary melt is required to explain the IA-rock compositions by bulk mixing, which is rather unlikely due to heat balance considerations. Therefore, either direct sediment entrapment into the mantle source and subsequent melting or post-melting crustal assimilation and simultaneous crystal fractionation (AFC) is required to explain the mixing relationships. To further constrain this, we modelled fractional crystallisation and combined crustal assimilation, applying the equations of DePaolo (1981). We used Th/Yb ratios vs. initial $^{143}Nd/^{144}Nd$ since Th is sensitive to sediment or crustal contamination due to its low concentration in primary depleted melts, and because Th is less affected by fluid-related mass transfer (Johnson and Plank 1999). Concentrations for Th and Yb in the contaminant were assumed to be represented by subducted sediment averages (6.5 ppm and 4.6 ppm; Plank and Langmuir 1998). Initial ϵ_{Nd} was varied between –10 and $+6$ to constrain the nature of the potential contami-

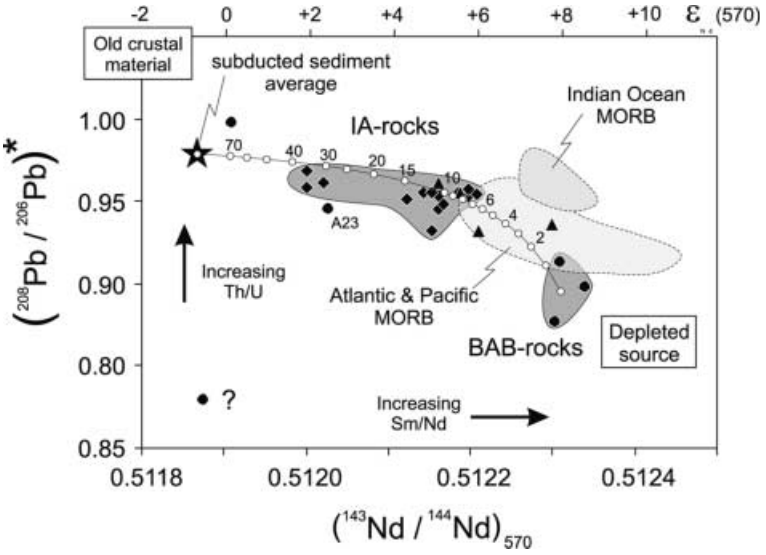

Fig. 12. Present-day radiogenic ($^{208}Pb/^{206}Pb$)* vs. initial $^{143}Nd/^{144}Nd$. ($^{208}Pb/^{206}Pb$)* was calculated by subtracting primordial Pb (Tatsumoto et al. 1973) from measured ratios: ($^{208}Pb/^{206}Pb$)* = ($^{208}Pb/^{204}Pb$–29.476)/($^{206}Pb/^{204}Pb$–9.307). High ($^{208}Pb/^{206}Pb$)* indicates a high, long-term Th/U of the source (or contaminant) and thus correlates with lower $^{143}Nd/^{144}Nd$. The IA rocks have lower $^{143}Nd/^{144}Nd$ and increased ($^{208}Pb/^{206}Pb$)* compared to the most depleted rocks (BAB rocks), indicating crustal contamination of the source or primary magma. The *line* denotes a bulk mixing line between a depleted melt (represented by the BAB pillow basalts) and average subducted sediment (*star*, data from Plank and Langmuir 1998; recalculated to 570 Ma), *numbers* give the amount of sediment (in %). Data for Atlantic, Pacific, and Indian Ocean MORB are from Ito et al. (1987), age corrected to 570 Ma using the depleted mantle $^{147}Sm/^{144}Nd$ of 0.2140. Symbols as in Fig. 11

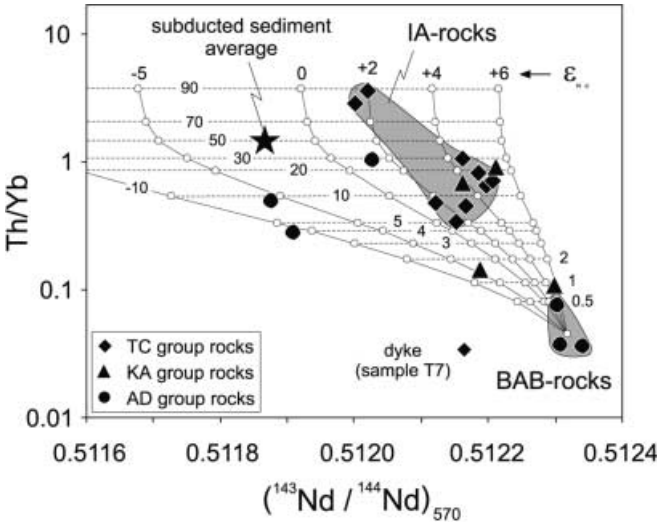

Fig. 13. Results of AFC calculations. Different curves represent different $^{143}Nd/^{144}Nd$ of assimilated material (*numbers* are ϵ_{Nd} values). *Stippled lines* are equilines and give the amount of mineral assemblage fractionated (consisting of 20 ol–40 cpx–40 plag, amount in %, partition coefficients from Bédard 1994; ratio of assimilation to fractionation: r = 0.8). Trace-element composition of assimilated material was assumed to be equal to average subducted sediments (data from Plank and Langmuir 1998). High Th/Yb ratios within the IA rocks require high amounts of assimilated crustal-like material (details see text)

nant. The results are shown in Fig. 13. The ratio of assimilation to fractionation (r parameter) must have been high assuming AFC processes (>0.8), since low ratios fail to explain the entire range in Th/Yb variation (lower r values do not affect the shape of the calculated curves but the absolute range in Th/Yb). The results further indicate that a large range in ϵ_{Nd} values of the assimilated material is necessary to explain all data points, and that the ϵ_{Nd} values were not lower than +2 to produce the IA rocks. Pre-existing Archaean or Proterozoic continental crust was therefore not involved during contamination. Although these considerations give some qualitative hints on the nature of the potential contaminant, and suggest that at least partly AFC processes may have taken place, we prefer the assumption of sediment entrapment into the mantle source and subsequent melting to be responsible for elevated ϵ_{Nd} values and Th enrichment within the IA rocks. This is because of the following reasons: (1) assuming solely AFC processes, the ϵ_{Nd} values of the assimilated material must have been highly heterogeneous (between at least 0 and +6), which is rather unlikely, (2) AFC processes require large amounts of crust to be assimilated (r = 0.8), which is inconsistent with the restricted range in Mg# of the IA rocks, (3) signatures of subducted sediments in volcanic rocks from many island-arc systems are a common feature (Patchett et al. 1984; White and Dupré 1986; Morris et al. 1990), and (4) because of the well-constrained correlation between ($^{208}Pb/^{206}Pb$)* vs. $^{143}Nd/^{144}Nd$ (Fig. 12). Adding sediments prior to melting will not change the calculated shape of the mixing curve in Fig. 12, but will lower the absolute amount of sediment necessary to produce the IA rocks to about 2–5% within the source.

Conclusions

The volcanic rocks of the Agardagh Tes-Chem ophiolite (ATCO) can be subdivided into three groups in terms of their trace-element and isotopic characteristics: (1) island-arc rocks (IA rocks) are characterised by enriched REE patterns, negative Nb anomalies, enrichment of LILE and intermediate initial ϵ_{Nd} values around +5.5; (2) back-arc basin-related rocks (BAB rocks) are characterised by flat REE patterns very similar to MORB, absent negative Nb anomalies but highly radiogenic initial ϵ_{Nd} values up to +8.5; (3) intermediate and exotic rocks with both highly depleted and enriched REE patterns but intermediate to low initial ϵ_{Nd} values down to –0.6. The island-arc and back-arc rocks are likely to be derived from the same depleted mantle source by different degrees of melting (2–3% and 8–15% respectively). Modification of the mantle wedge by subducted sediments combined with mixing processes superimposed to crystal fractionation is suitable to explain most of the trace-element and isotopic data.

Based on these results, we suggest the evolution of the ATCO as part of an intra-oceanic island-arc back-arc system. The IA rocks represent early-stage volcanic rocks of a young arc system, in which fluids and probably melts released from the downgoing slab initiated low-degree melting of a mantle wedge previously modified by accreted sediments. This led to highly enriched IA rocks with intermediate initial ϵ_{Nd} values. The preservation of isotopic and trace-element heterogeneities within this suite of rocks implies poor mixing between different melt batches on their way to the surface. Although speculative, this may also indicate a restricted thickness of the overlying crust, in which storage and mixing of different magma batches is difficult to achieve. Therefore, this crust may have been pre-existing oceanic crust rather than continental crust. We further suggested that, simultaneous to the formation of the IA rocks, the BAB rocks were formed in the back-arc region from the same depleted mantle source, but without the influence of slab-derived components. These rocks are therefore more depleted in highly incompatible trace elements and are highly radiogenic in $^{143}Nd/^{144}Nd$. This requires a hot, upwelling depleted mantle in the back-arc region to provide sufficient heat to produce these melts.

Acknowledgements We thank V. Lebedev, C. Oidup, A. Songorakova, and A. Kotov for their substantial logistic support during the field season in 1997. P. Maissenbacher, B. Stoll and M. Hofmann assisted during SSMS analyses. I. Raczek and H. Feldmann provided substantial help during isotope chemistry and mass spectrometry, and W. Abouchami and S. Galer during the Pb–Pb triple spike analyses. Discussions with S. Jung, E. Hellebrand, A. Sassen and M. Kurth improved the manuscript considerably. Reviews by T.F. Kokfelt and an anonymous reviewer are gratefully acknowledged. J.P. particularly thanks A. Hofmann for providing access to the facilities at MPI and for numerous encouraging discussions. This work was funded by Deutsche Forschungsgemeinschaft grant Kr 590/61-1 to A.K. and is part of the first author's doctoral thesis. I.K. was funded by RFFI 99-05-65337.

Appendix: Analytical methods

Major elements and Ba, Y, Sc, V, Cr, Co, Ni, Cu, Zn, and Ga were determined on a Philips PW 1404 X-ray fluorescence spectrometer at Universität Mainz using common XRF techniques on fused and powder pellets. Reproducibility is better than 1% for major elements and better than 4% for trace elements. FeO was calculated from Fe_2O_3 assuming that all iron was Fe^{II}. All other trace elements (except Rb, Sr, Sm, and Nd) were determined either by isotope dilution multi-ion counting spark-source mass spectrometry at the Max-Planck-Institut für Chemie in Mainz (MIC-SSMS; Jochum et al. 1997) or by ICP-MS at Memorial University in St. Jones, Newfoundland, Canada, following the technique of Jenner et al. (1990). For the MIC-SSMS measurement of very low Zr and Nb concentrations in Al-rich samples, a special procedure was necessary to correct for isobaric interferences. This procedure includes a high mass resolution (~3,000) and a mathematical interference correction, and yields an analytical precision of 2–5% for concentrations down to 0.02 ppm and 10% for lower concentrations (Pfänder et al. 1999). For all other trace elements, the precision of the MIC-SSMS technique is within 3–5% of the recommended values for international reference materials for elements determined by isotope dilution, and within 10% for elements determined by the internal standard procedure (Jochum et al. 1988). The precision of the ICP-MS analyses is given to be better than 10%.

Nd, Sr, and Pb isotopic compositions were measured on Finnigan MAT 261 multicollector thermal ion-source mass spectrometers in static mode. Nd and Sr isotopic analyses and Nd, Sm, Sr, and Rb concentrations were analysed on the same sample powder using mixed ^{150}Nd–^{149}Sm and ^{84}Sr–^{85}Rb spikes. After spiking, the sample powder was dissolved in HF–HNO_3 in closed Teflon beakers for >48 h at 200 °C. Rb, Sr and REE were separated on Bio-Rad AG 50W-X12 cation-exchange resin. From the REE fraction, Sm and Nd were subsequently separated using HDEHP-coated Teflon powder. Total procedural blanks were <500 pg for Sr and <30 pg for Nd. Measured Sr isotopic ratios were normalised to $^{86}Sr/^{88}Sr = 0.1194$, Nd isotopic ratios to $^{146}Nd/^{144}Nd = 0.7219$. Repeated measurements of the NBS 987 Sr standard resulted in $^{87}Sr/^{86}Sr = 0.710212 \pm 0.000036$ and $^{84}Sr/^{86}Sr = 0.056495 \pm 0.000053$ (errors 2σ, $N = 10$). Repeated measurements of the La Jolla Nd standard gave $^{143}Nd/^{144}Nd = 0.511839 \pm 0.000025$, $^{145}Nd/^{144}Nd = 0.348402 \pm 0.000017$ and $^{150}Nd/^{144}Nd = 0.236478 \pm 0.000082$ (2σ, $N = 33$). Pb was isolated from hand-picked rock chips up to 200 mg by weight. After leaching in hot 6 M HCl for several hours and rinsing in ultrapure water, the chips were dissolved in closed Teflon beakers using hot HF–HNO_3 for >48 h. Pb separation was carried out on Bio-Rad AG1-X8 anion-exchange resin using a HBr–HCl procedure. Total procedural blanks are <200 pg. Mass fractionation was determined by repeated measurements

of the NBS 981 Pb standard for each batch of samples and was between 1.02 ± 0.20 and $1.32 \pm 0.05‰$ per amu ($\pm 2\sigma$). Measured ratios of the NBS 981 Pb standard were $^{208}Pb/^{204}Pb = 36.696 \pm 0.049$, $^{207}Pb/^{204}Pb = 15.490 \pm 0.015$, $^{206}Pb/^{204}Pb = 16.933 \pm$ z0.012, $^{207}Pb/^{206}Pb = 0.91481 \pm 0.00030$ ($\pm 2\sigma$, N = 10, corrected for fractionation). Selected samples were re-measured for Pb isotopic composition by using the highly precise triple spike technique (Galer 1999). This technique requires the run of spiked and unspiked sample aliquots to correct for instrumental mass fractionation but improves the accuracy of the isotopic ratios by at least a factor of 10. Sample dissolution was similar to the procedure described above, but separation was done on AG1-X8 resin using a diluted $HBr–HNO_3$ eluent to improve purity and blank on eluted Pb. Total procedural blanks using this technique were between 8 and 40 pg.

References

Albarède F (1995) Introduction to geochemical modeling. Cambridge University Press, Cambridge

Avdeyev AV (1984) Ophiolite zones and the geological history of Kazakhstan from the mobilistic standpoint. Int Geol Rev 26:995–1004

Bédard JH (1994) A procedure for calculating the equilibrium distribution of trace elements among the minerals of cumulate rocks, and the concentration of trace elements in the coexisting liquids. Chem Geol 118:143–153

Belichenko VG, Sklyarov EV, Dobretsov NL, Tomurtogoo O (1994) Geodynamic map of Paleoasian ocean: eastern segment. Russian Geol Geophys 35:23–32

Berzin NA, Coleman RG, Dobretsov NL, Zonenshain LP, Xuchang X, Chang EZ (1994) Geodynamic map of the western part of the Paleoasian ocean. Russian Geol Geophys 35:5–22

Brenan JM, Shaw HF, Phinney DL, Ryerson FJ (1994) Rutile-aqueous fluid partitioning of Nb, Ta, Hf, Zr, U and Th: implications for high field strength element depletion in island-arc basalts. Earth Planet Sci Lett 128:327–339

Buchan C, Cunningham D, Windley BF, Tomurhuu D (2001) Structural and lithological characteristics of the Bayankhongor Ophiolite Zone, central Mongolia. J Geol Soc Lond 158:445–460

Chauvel C, Hofmann AW, Vidal P (1992) HIMU-EM: the French-Polynesian connection. Earth Planet Sci Lett 110:99–119

Coleman RG (1989) Continental growth of northwest China. Tectonics 8:621–635

Conrad WK, Kay RW (1984) Ultramafic and mafic inclusions from Adak Island: crystallization history, and implications for the nature of primary magmas and crustal evolution in the Aleutian Arc. J Petrol 25:88–125

Davies JH, Bickle MJ (1991) A physical model for the volume and composition of melt produced by hydrous fluxing above subduction zones. Philos Trans R Soc Lond 335:355–364

DePaolo DJ (1981) Trace-element and isotopic effects of combined wallrock assimilation and fractional crystallization. Earth Planet Sci Lett 53:189–202

Didenko AN, Mossakovskii AA, Pecherskii DM, Ruzhentsev SV, Samygin SG, Kheraskova TN (1994) Geodynamics of the central-Asian Paleozoic oceans. Russian Geol Geophys 35:48–61

Doe BR, Zartman RE (1979) Plumbotectonics, the Phanerozoic. In: Barnes HL (ed) Geochemistry of hydrothermal ore deposits, Wiley Interscience, New York, pp 22–70

Eissen JP, Lefevre C, Maillet P, Morvan G, Nohara M (1991) Petrology and geochemistry of the central north Fiji basin spreading center (southwest Pacific) between 16 degrees and 22 degrees. Mar Geol 98:201–239

Elliot T, Plank T, Zindler A, White W, Bourdon B (1997) Element transport from slab to volcanic front at the Mariana arc. J Geophys Res 102:14991–15019

Ez VV (1983) Correlation of endogenous processes and their role in the early Precambrian crustal development of southern east Siberia. In: Rast N, Delany FM (eds) Profiles of orogenic belts. AGU Geodynamic Series 10, pp 145–204

Fedorovskii VS, Khain EV, Vladimirov AG, Kargopolov SA, Gibsher AS, Izokh AE (1995) Tectonics, metamorphism, and magmatism of collisional zones of the Central Asian Caledonides. Geotectonics 29:193–212

Frey FA, Green DH, Roy SD (1978) Integrated models of basalt petrogenesis: a study of quartz tholeiites to olivine melilitites from South Eastern Australia utilizing geochemical and experimental petrological data. J Petrol 19:463–513

Galer SJG (1999) Optimal double and triple spiking for high precision lead isotopic measurement. Chem Geol 157:255–274

Galer SJG, O'Nions RK (1985) Residence time of thorium, uranium and lead in the mantle with implications for mantle convection. Nature 316:778–782

Goldstein S, O'Nions RK, Hamilton PJ (1984) A Sm-Nd isotopic study of atmospheric dusts and particulates from major river sediments. Earth Planet Sci Lett 70:221–236

Hawkesworth CJ, Turner SP, McDermott F, Peate DW, van Calsteren P (1997) U-Th isotopes in arc magmas: implications for element transfer from the subducted crust. Science 276:551–555

Hawkins JW Jr (1976) Petrology and geochemistry of basaltic rocks of the Lau Basin. Earth Planet Sci Lett 28:283–297

Hawkins JW, Melchior JT (1985) Petrology of Mariana trough and Lau basin basalts. J Geophys Res 90:11431–11468

Heath E, Macdonald R, Belkin H, Hawkesworth C, Sigurdsson H (1998) Magmagenesis at Soufriere Volcano, St. Vincent, Lesser Antilles Arc. J Petrol 39:1721–1764

Hess PC (1992) Phase equilibria constraints on the origin of ocean floor basalts. Geophys Monogr 71:67–102

Hofmann AW (1988) Chemical differentiation of the Earth: the relationship between mantle, continental crust, and oceanic crust. Earth Planet Sci Lett 90:297–314

Hofmann AW (2001) Lead isotopes and the age of the Earth – a geochemical accident. In: Lewis CLE, Knell SJ (eds) The age of the Earth: from 4004 BC to AD 2002. Geol Soc London, Spec Pub 190, pp 223–236

Ilyn AV (1990) Proterozoic supercontinent, its latest Precambrian rifting, breakup, dispersal into smaller continents, and subsidence of their margins: evidence from Asia. Geology 18:1231–1234

Ionov DA, Hofmann AW (1995) Nb-Ta-rich mantle amphiboles and micas: Implications for subduction-related metasomatic trace element fractionations. Earth Planet Sci Lett 131:341–356

Ito E, White WM, Göpel C (1987) The O, Sr, Nd and Pb isotope geochemistry of MORB. Chem Geol 62:157–176

Jacobsen SB, Kaufman AJ (1999) The Sr, C and O isotopic evolution of Neoproterozoic seawater. Chem Geol 161:37–57

Jenner GA, Longerich HP, Jackson SE, Fryer BJ (1990) ICP-MS-A powerful tool for high-precision trace-element analysis in earth sciences – evidence from analysis of selected USGS reference samples. Chem Geol 83:133–148

Jochum KP, Seufert HM, Midinet-Best S, Rettmann E, Schönberger K, Zimmer M (1988) Multi-element analysis by isotope dilution-spark source mass spectrometry (ID-SSMS). Fresenius J Anal Chem 331:104–110

Jochum KP, Laue HJ, Seufert HM, Dienemann C, Stoll B, Pfänder J, Flanz M, Achtermann H, Hofmann AW (1997) Multi-ion counting-spark source mass spectrometry (MIC-SSMS): a new multielement technique in geo- and cosmochemistry. Fresenius J Anal Chem 359:385–389

Johnson KTM (1998) Experimental determination of partition coefficients for rare earth and high-field-strength elements between clinopyroxene, garnet, and basaltic melt at high pressure. Contrib Mineral Petrol 133:60–68

Johnson MC, Plank T (1999) Dehydration and melting experiments constrain the fate of subducted sediments. Geochem Geophys Geosyst 1

Kelemen PB (1990) Reaction between ultramafic rock and fractionating basaltic magma I. phase relations, the origin of calc-alkaline magma series, and the formation of discordant dunite. J Petrol 31:51–98

Kelemen PB, Johnson KTM, Kinzler RJ, Irving AJ (1990) High-field strength element depletions in arc basalts due to mantle-magma interaction. Nature 345:521–524

Kepezhinskas KB (1986) Structural-metamorphic evolution of late Proterozoic ophiolites and Precambrian basement in the central Asian foldbelt of Mongolia. Precambrian Res 33:209–223

Kepezhinskas PK, Kepezhinskas KB, Puchtel IS (1991) Lower Paleozoic oceanic crust in Mongolian Caledonides: Sm-Nd isotope and trace element data. Geophys Res Lett 18:1301–1304

Khain EV, Bibikova EV, Degtyarev KE (1999) The Paleo-Asian ocean in the Neoproterozoic and early Palaeozoic: new radiometric data (in Russian). In: Geological history of the Proterozoic marginal Palaeoceanic structures of northern Eurasia. Tema, St Petersburg, pp 175–181

Khain VE, Gusev GS, Khain EV, Vernikovskym VA, Volobuyev MI (1997) Circum-Siberian Neoproterozoic ophiolite belt. Ofioliti 22:195–200

Kovalenko VI, Pukhtel IS, Yarmolyuk VV, Zhuravlev DZ, Stosch H, Jagoutz E (1996a) The Sm-Nd isotopic systematics of ophiolites in the Ozernaya Zone (Mongolia). Stratigr Geol Correlation 4:107–113

Kovalenko VI, Yarmolyuk VV, Kovach VP, Kotov AB, Kozakov IK, Salnikova EB (1996b) Sources of Phanerozoic granitoids in central Asia: Sm–Nd isotope data. Geochem Int 34:628–640

Kozakov IK (1986) Precambrian infracrustal complexes of Mongolia (in Russian). Nauka Publ House, Leningrad

Kuzmichev AB, Bibikova EV, Zhuralev DZ (2001) Neoproterozoic (~800 Ma) orogeny in the Tuva-Mongolia massif (Siberia): island arc-continent collision at the northeast Rodiniaq margin. Precambrian Res 110:109–126

Ludden J, Geliens L, Trudel P (1982) Archean metavolcanics from the Rouyin-Noranda district, Abitibi greenstone belt, Quebec. 2. Mobility of trace elements and petrogenetic constraints. Can J Earth Sci 19:2276–2287

McKenzie D, O'Nions RK (1991) Partial melt distributions from inversion of rare earth element concentrations. J Petrol 32:1021–1091

McKenzie D, O'Nions RK (1995) The source regions of ocean island basalts. J Petrol 36:133–159

Melnikov AI, Mazukabzov AM, Sklyarov EV, Vasiliev EP (1994) Baikal rift basement: structure and tectonic evolution. Bull Centr Rech Explor Prod Elf Aquitaine 18:99–122

Mitrofanov FP, Kozakov IK (1993) Precambrian in younger fold belts. In: Rundqvist DV, Mitrofanov FP (eds) Precambrian geology of the USSR. Elsevier, Amsterdam, pp 443–498

Morris JD, Leeman WP, Tera F (1990) The subducted component in island arc lavas: constraints from Be isotopes and B-Be systematics. Nature 344:31–36

Mossakovsky AA, Ruzhentsev SV, Samygin SG, Kheraskova TN (1993) The Central Asian fold belt: geodynamic evolution and formation history. Geotectonics 6:3–32

Münker C (2000) The isotope and trace element budget of the Cambrian Devil River arc system, New Zealand: identification of four source components. J Petrol 41:759–788

Navon O, Stolper E (1987) Geochemical consequences of melt percolation – the upper mantle as a chromatographic column. J Geol 95:285–307

Patchett PJ, White WM, Feldmann H, Kielinczuk S, Hofmann AW (1984) Hafnium/rare earth element fractionation in the sedimentary system and crustal recycling into the Earth's mantle. Earth Planet Sci Lett 69:365–378

Peacock SM (1993) Large-scale hydration of the lithosphere above subducting slabs. Chem Geol 108:49–59

Peacock SM, Rushmer T, Thompson AB (1994) Partial melting of subducting oceanic crust. Earth Planet Sci Lett 121:227–244

Pearce JA, Ernewein M, Bloomer SH, Parson LM, Murton BJ, Johnson LE (1995) Geochemistry of Lau basin volcanic rocks: influence of ridge segmentation and arc proximity. Geol Soc Lond Spec Publ 81:53–75

Pearce JW, Peate DW (1995) Tectonic implications of the composition of volcanic arc magmas. Annu Rev Earth Planet Sci 23:251–285

Pedersen RB, Dunning GR (1997) Evolution of arc crust and relations between contrasting sources: U-Pb (age), Nd and Sr isotope systematics of the ophiolite terraine of SW Norway. Contrib Mineral Petrol 128:1–15

Pfänder JA, Jochum KP, Kröner A, Kozakov I, Oidup C, Todt W (1998) Age and geochemical evolution of an early Cambrian ophiolite-island arc system in Tuva, South Central Asia. In: Generation and emplacement of ophiolites through time. Geol Surv Finland Spec Pap 26:42

Pfänder JA, Jochum KP, Sassen A, Stoll B, Maissenbacher P, Murmann M (1999) Determination of Y, Zr and ultra-low Nb concentrations in geological material by multi-ion counting spark-source mass spektrometry (MIC-SSMS). Fresenius J Anal Chem 364:376–380

Plank T, Langmuir CH (1998) The chemical composition of subducting sediment and its consequences for the crust and mantle. Chem Geol 145:325–394

Presnall DC, Hoover JD (1987) High pressure phase equilibrium constraints on the origin of mid-ocean ridge basalts. In: Mysen BO (ed) Magmatic processes: physicochemical principles. Spec Publ Geochem Soc, St Louis, pp 75–89

Rapp RP, Shimizu N, Norman MD, Applegate GS (1999) Reaction between slab-derived melts and peridotite in the mantle wedge: experimental constraints at 3.8 GPa. Chem Geol 160:335–356

Regelous M, Collerson KD, Ewart A, Wendt JI (1997) Trace element transport rates in subduction zones: evidence from Th, Sr and Pb isotope data for Tonga-Kermadec arc lavas. Earth Planet Sci Lett 150:291–302

Ryan J, Morris J, Bebout G, Leeman B (1996) Describing chemical fluxes in subduction zones: insights from "depth-profiling" studies of arc and forearc rocks. Geophys Monogr 96:263–268

Ryerson FJ, Watson EB (1987) Rutile saturation in magmas: implications for Ti-Nb-Ta depletion in island-arc basalts. Earth Planet Sci Lett 86:225–239

Salnikova EB, Kozakov IK, Kotov AB, Kröner A, Todt W, Nutman A, Yakovleva SZ, Kovach VP (2001) Age of Palaeozoic granites and metamorphism in the Tuvino-Mongolian massif of the central Asian mobile belt: loss of a Precambrian microcontinent. Precambrian Res 110:143–164

Sengör AMC, Okurogullari AH (1991) The role of accretionary wedges in the growth of continents: Asiatic examples from Argand to plate tectonics. Eclogae Geol Helv 84:535–597

Sengör AMC, Natal'in BA, Burtman VS (1993) Evolution of the Altaid tectonic collage and Palaeozoic crustal growth in Eurasia. Nature 364:299–307

Shaw DM (1970) Trace element fractionation during anatexis. Geochim Cosmochim Acta 34:237–243

Shervais JW (1982) Ti-V plots and the petrogenesis of modern and ophiolitic lavas. Earth Planet Sci Lett 59:101–118

Stacey JS, Kramers JD (1975) Approximation of terrestrial lead isotope evolution by a two-stage model. Earth Planet Sci Lett 26:207–221

Staudigel H, Plank T, White B, Schmincke H-U (1996) Geochemical fluxes during seafloor alteration of the basaltic upper oceanic crust: DSDP sites 417 and 418. Geophys Monogr 96:19–38

Stein M, Hofmann AW (1994) Mantle plumes and episodic crustal growth. Nature 372:63–68

Stolper E, Newman S (1994) The role of water in the petrogenesis of the Mariana trough magmas. Earth Planet Sci Lett 121:293–325

Sun Ss, McDonough WF (1989) Chemical and isotopic systematics of oceanic basalts: implications for mantle compositions and processes. Geol Soc Spec Publ 42:313–345

Swinden HS, Jenner GA, Fryer BJ, Hertogen J, Roddick JC (1990) Petrogenesis and paleotectonic history of the Wild Bight

Group, an Ordivician rifted island arc in Central Newfoundland. Contrib Mineral Petrol 105:219–241
Tatsumi Y (1989) Migration of fluid phases and genesis of basalt magmas in subduction zones. J Geophys Res 94:4697–4707
Tatsumoto M, Knight RJ, Allègre CJ (1973) Time differences in the formation of meteorites as determined from the ratio of lead-207 to lead-206. Science 180:1279–1283
Thirlwall MF, Graham AM (1984) Evolution of high-Ca, high-Sr C-series basalts from Grenada, Lesser Antilles: the effects of intra-crustal contamination. J Geol Soc Lond 141:427–445
White WM, Dupré B (1986) Sediment subduction and magma genesis in the Lesser Antilles: isotopic and trace element constraints. J Geophys Res 91:5927–5941
Woodhead J, Eggins S, Gamble J (1993) High field strength and transition element systematics in island arc and back-arc basin basalts: evidence for multi-phase melt extraction and a depleted mantle wedge. Earth Planet Sci Lett 114:491–504
Woodhead JD, Eggins SM, Johnson RW (1998) Magma genesis in the New Britain island arc: further insights into melting and mass transfer processes. J Petrol 39:1641–1668
Zimmer M, Kröner A, Jochum KP, Reischmann T, Todt W (1995) The Gabal Gerf complex: a Precambrian N-MORB ophiolite in the Nubian Shield, NE Africa. Chem Geol 123:29–51
Zonenshain LP, Kuzmin MI (1978) The Khan-Taishir ophiolitic complex of western Mongolia, its petrology, origin and comparison with other ophiolitic complexes. Contrib Mineral Petrol 67:95–109
Zonenshain LP, Kuzmin MI, Natapov LM (1990) Geology of the USSR: a plate-tectonic synthesis. AGU Geodynamics Series 21